# Applicability of the Zintl concept to understanding the crystal chemistry of lithium-rich germanides and stannides

Kowsik Ghosh<sup>1</sup>, Salina Rahman<sup>1</sup>, Alexander Ovchinnikov<sup>1,2</sup>, and Svilen Bobev<sup>1,\*</sup>

<sup>&</sup>lt;sup>1</sup> Department of Chemistry and Biochemistry, University of Delaware, Newark, Delaware 19716, United

States

<sup>&</sup>lt;sup>2</sup> Faculty of Chemistry and Food Chemistry, Technische Universität Dresden, 01062 Dresden, Germany

#### **ABSTRACT**

With this contribution, we take a new, critical look at the structures of the binary phases Li<sub>5</sub>Ge<sub>2</sub> and  $\text{Li}_5\text{Sn}_2$ . Both are isostructural (centrosymmetric space group  $R\overline{3}m$ , no. 166), and in their structures, all germanium (tin) atoms are dimerized. Application of the valence rules will require the allocation of six additional valence electrons per [Ge<sub>2</sub>] or [Sn<sub>2</sub>] unit considering single covalent bonds, akin to those in the dihalogen molecules. Alternatively, four additional valence electrons per [Ge2] or [Sn2] anion will be needed if homoatomic double bonds exist, in an analogy with dioxygen. Therefore, five lithium atoms in one formula unit cannot provide the exact number of electrons, leaving open questions as to what is the nature of the chemical bonding within these moieties. Additionally, by means of single-crystal X-ray diffraction, synchrotron powder X-ray diffraction, and neutron powder diffraction, we established that the Li and Sn atoms in Li<sub>5</sub>Sn<sub>2</sub> are partially disordered, i.e., the actual chemical formula of this compound is  $\text{Li}_{5-x}\text{Sn}_{2+x}$  (0 < x < 0.1). The convoluted atomic bonding in the case where tin atoms partially displace lithium atoms results in the formation of larger covalently bonded fragments. Our first-principle calculations suggest that such disorder leads to electron doping. Contrary to that, both experimental and computational findings indicate that in the Li<sub>3</sub>Ge<sub>2</sub> structure, the [Ge<sub>2</sub>] dimers are slightly oxidized, i.e., hole-doped, as a result of approx. 30% vacancies on a Li site, i.e., the actual chemical formula of this compound is  $\text{Li}_{5-x}\text{Ge}_2$  ( $x \approx 0.3$ ).

#### 1. INTRODUCTION

Since the turn of the 21<sup>st</sup> century, lithium-ion batteries (LIBs) have become one of the most important energy storage technologies.<sup>1-11</sup> To meet the increasing requirements of electromobility, the workhorse graphite-based anodes with a maximum capacity of 372 mAh g<sup>-1</sup> need to be replaced by materials with an increased specific lithium uptake.<sup>3</sup> To this end, lithium phases with heavier group 14 elements (tetrel = *Tt*) become attractive candidates for the development of new anode materials.<sup>3,12,13</sup> Since Li–Si materials suffer from volume expansion during cycling,<sup>14-18</sup> Li–Ge/Sn phases emerge as more promising candidates for LIBs applications. Yet, to conceive and ultimately make better anode materials, we need to better understand the structural chemistry of the various Li–Ge and Li–Sn phases that will form upon lithiation of Ge- and Sn-based anodes.

The introductory part of this article is the rightful place to provide a brief recap of the historical developments with regard to the Li–Ge and Li–Sn binaries. The first reports date back to the 1950s and cover compounds/structures that have been since corrected (e.g., Li<sub>3</sub>Ge, Li<sub>4</sub>Ge) <sup>19</sup>. In subsequent years, more binary germanides were identified, including LiGe,<sup>20</sup> Li<sub>9</sub>Ge<sub>4</sub>,<sup>21</sup> Li<sub>7</sub>Ge<sub>2</sub>,<sup>22</sup> Li<sub>11</sub>Ge<sub>6</sub>,<sup>23</sup> Li<sub>7</sub>Ge<sub>12</sub>,<sup>24</sup> Li<sub>4.096</sub>Ge,<sup>25</sup> Li<sub>17</sub>Ge<sub>4</sub>,<sup>26</sup> Li<sub>15</sub>Ge<sub>4</sub>,<sup>27,28</sup> Li<sub>12</sub>Ge<sub>7</sub>,<sup>29</sup> and Li<sub>5</sub>Ge<sub>2</sub> <sup>30</sup>. Most binary stannides were worked out in the 1960s and 1970s, including Li<sub>2</sub>Sn<sub>5</sub>,<sup>31</sup> LiSn,<sup>32</sup> Li<sub>7</sub>Sn<sub>3</sub>,<sup>33</sup> Li<sub>5</sub>Sn<sub>2</sub>,<sup>34</sup> Li<sub>7</sub>Sn<sub>2</sub>,<sup>35</sup> Li<sub>13</sub>Sn<sub>5</sub>,<sup>36</sup> and Li<sub>22</sub>Sn<sub>5</sub>.<sup>37</sup> The latter was reformulated as Li<sub>17.05</sub>Sn<sub>4</sub> in 2001,<sup>25</sup> with the revised structure independently confirmed by neutron powder diffraction studies <sup>38</sup>. Very recently, Li<sub>5</sub>Sn was reported as the binary tetrelide with the highest amount of lithium so far <sup>39</sup>.

The structures of all of the mentioned binaries are found in the ICSD crystallographic database, however, the reader is cautioned that there are still controversies surrounding them. For example, crystal structure of Li<sub>2</sub>Sn<sub>5</sub> is now understood to be the revised structure of the phase that was previously reported as LiSn<sub>2</sub><sup>31</sup>. The cubic structure of Li<sub>21</sub>Ge<sub>5</sub> (also referred to as Li<sub>22</sub>Ge<sub>5</sub>) was redetermined by Nazar *et al.* in 2001 <sup>26</sup> and also reinvestigated by Fässler *et al.* <sup>25</sup> The revisions of the structure noted that the earlier

reports with partially occupied Li sites could not be replicated. Very near the "17:4" composition, another lithium-rich phase, Li<sub>24.1</sub>Ge with an orthorhombic crystal structure, was identified and structurally characterized not too long ago.<sup>25</sup> Computational work, however, indicates a different ground state for Li<sub>4</sub>Ge <sup>40</sup>, with the possibility for pressure-induced phase transition. Following that, two other high pressure LiGe phases in space group *I4*<sub>1</sub>/*amd* and space group *P6*<sub>3</sub>/*mmc* were revisited by Evers *et al.* <sup>41</sup>.

There also exist discrepancies in the literature due to "assignment" of structures. For example, in analogy with the previously known Li<sub>7</sub>Si<sub>2</sub> <sup>42</sup> that had been reformulated as Li<sub>13</sub>Si<sub>4</sub> <sup>43,44</sup> (Li<sub>7</sub>Si<sub>2</sub> = Li<sub>14</sub>Si<sub>4</sub>, where partially occupied Li sites change the formula to Li<sub>13</sub>Si<sub>4</sub>), Nesper *et al.* suggested the existence of Li<sub>13</sub>Ge<sub>4</sub>. However, full crystallographic details confirming Li<sub>13</sub>Ge<sub>4</sub> are still missing. Grüttner *et al.*, <sup>23</sup> upon redetermination of the Li–Ge phase diagram, noted that the phase Li<sub>11</sub>Ge<sub>6</sub> could not be synthesized as a part of their work. Easter, Fässler *et al.* opined that the structure of Li<sub>11</sub>Ge<sub>6</sub> is "strikingly similar" to that of Li<sub>8</sub>MgSi<sub>6</sub> <sup>46</sup>, alluding to the possibility that it might be the structure of Li<sub>8</sub>MgGe<sub>6</sub> which has erroneously been assigned as Li<sub>11</sub>Ge<sub>6</sub>. Technological advancements of the crystallographic instrumentation and methods over the last few decades could provide the sought after clarity, although it is recognized that due to its only three electrons, more accurate description of the lithium positions/occupancies may not be possible, especially in cases where lithium atoms can be mobile within the structure.

In this paper, we describe our attempts to fully understand the rhombohedral crystal structure of  $\text{Li}_5\text{Ge}_2$ , first identified during the de/lithiation work of the  $\text{Ba}_8\text{Ge}_{43}$  type-I clathrate, done by in-situ synchrotron X-ray diffraction <sup>30</sup>. Prior to that,  $\text{Li}_5\text{Ge}_2$  was only suggested from computational work by Morris *et al.*,<sup>47</sup> as a phase near the bottom of a convex hull and in close proximity to another hitherto unknown binary phase, the hexagonal  $\text{Li}_7\text{Ge}_3$ . Although in reference 30, we did a Rietveld refinement and confirmed the structure of  $\text{Li}_5\text{Ge}_2$ , follow up work on the direct synthesis of this phase indicated that the unit cell parameters vary slightly from sample to sample. Specifically, we note the observation that there is a large variability of the *c*-axis parameter, from c = 18.396(9) Å, matching perfectly the previously reported c = 18.396(9) Å, matching perfectly the previously reported c = 18.396(9) Å, matching perfectly the previously reported c = 18.396(9) Å.

18.397(1) Å,<sup>30</sup> to a value as low as 18.324(2) Å. These results indicate that Li<sub>5</sub>Ge<sub>2</sub>, most likely, is not a line compound, a case that could be analogous to Li<sub>5</sub>Si<sub>2</sub>, which von Schnering *et al.* showed to host Li defects.<sup>48</sup> The existence of Ge defects is another possibility; the hypothesis that the homogeneity range can be due to Li/Ge disorder is also a viable alternative, brought to light by the demonstration that lithium atoms can share position with germanium atoms in some structures, such as Ba<sub>8</sub>Li<sub>x</sub>Ge<sub>46-x</sub> (x < 5.33), <sup>49</sup> and Ba<sub>2</sub>Li<sub>1-x</sub>Ge<sub>3+x</sub> (x < 0.1). <sup>50</sup>

To distinguish the eventual scenarios  $\text{Li}_{5-x}\text{Ge}_{2+x}$  vs  $\text{Li}_{5-x}\text{Ge}_2$ , we decided to reinvestigate the isotypic  $\text{Li}_5\text{Sn}_2$  phase as well, employing the same techniques—single-crystal X-ray diffraction for multiple crystals, supported by the Rietveld refinement of synchrotron X-ray powder diffraction and neutron powder diffraction data. The results from the structural work are discussed in the context of the Zintl concept,  $^{51,52}$  which also proves helpful in rationalizing the structures. Electronic band structure calculations by means of the LMTO methods are also presented and discussed.

# 2. EXPERIMENTAL SECTION

## 2.1 Synthesis.

Samples of  $\text{Li}_{5-x}Tt_{2+x}$  (x < 0.2) (Tt = Ge and Sn) were prepared by fusing the elements together in either an induction furnace or a regular tube furnace. All work was carried out under protective atmosphere (argon gas-filled glovebox with  $O_2/H_2O$  levels below 1 ppm) or under vacuum, since both the starting materials and the products are unstable in air. The elements Li, Sn and Ge were purchased from Sigma-Aldrich and Alfa Aesar with a purity  $\geq 99.9$  %wt. The surface of Li rod was cleaned with a scalpel blade immediately before use. The elements were taken in several different ratios close to the stoichiometric 5:2. The elemental mixtures (approx. 0.4-0.5 g in total) were then put into Nb-tubes (1.6-1.7 inch long, 0.375 inch diameter) that were previously welded on one side. After the elements were loaded, the tubes were subsequently welded shut (under argon atmosphere). The closed niobium tubes were then put into

evacuated fused silica tubes and heat-treated. All the reactions were carried out under identical conditions. For the germanium samples, using an induction furnace, the following temperature profile was found to work the best: heating to 923 K (for 30 sec)  $\rightarrow$  1123 K (for 30 sec)  $\rightarrow$  1223 K (for 30 sec)  $\rightarrow$  1273 K (for 8 min)  $\rightarrow$  1023 K (30 sec), before the furnace was switched off and the specimens cooled to room temperature. An IR pyrometer was used to measure temperature. For the tin samples, the steps were as follow: heating to 923 K (for 30 sec)  $\rightarrow$  973 K (for 30 sec)  $\rightarrow$  1023 K (for 10 min), before the furnace was switched off and the specimens cooled to room temperature. When tube furnace was used, the samples were heated to 1273 K (rate of 100 K/h) for 2 hours, and then cooled to room temperature with a 25 K/h cooling rate. Then, the welded tubes were brought back in the glove box and cut open to recover the products.

# 2.2. Single-crystal X-ray diffraction (SCXRD)

Several crystals from different batches were used for the SCXRD experiments. For this purpose, suitable single-crystals were selected in the glove box, and were cut under dry Paratone-N oil to dimensions  $\leq 0.10$  mm. After that, the crystals were scooped by MiTeGen plastic loops and transferred to the goniometer of a Bruker APEX II diffractometer, equipped with monochromatized Mo K $\alpha$  radiation,  $\lambda$  = 0.71073 Å. Data acquisitions were done at 200(2) K, maintained by a stream of cold nitrogen gas. Data sets were processed with the SAINT and SADABS software packages. Structure solutions via direct methods were tried in all possible space groups: the chiral R3 and R32, the non-centrosymmetric R3m, and the centrosymmetric R3m without significant differences. Therefore, the latter was chosen. Inspections of the data showed no evidence for the existence of spots that can be indexed to unit cells with larger volumes/lower symmetry. Refinements were done by full-matrix least-squares minimizations on  $F^2$  and were carried out with either SHELXL  $^{53,54}$  or WinCSD.  $^{55}$  In the final stages, atomic coordinates and labels were set to be consistent with previous studies  $^{34}$ . It is important to note here that in almost all

structures, every atom in the structure was refined with an anisotropic displacement parameter, including Li. Only in one of the cases where Li occupancy was refined, the displacement parameter of that atom had to be treated as isotropic.

CCDC numbers 2340451 to 2340457 contain the full supplementary crystallographic data for the compounds discussed in this paper. CIF files can be obtained free of charge via www.ccdc.cam.ac.uk/data\_request/cif, or by emailing data\_request@ccdc.cam.ac.uk, or by contacting The Cambridge Crystallographic Data Centre, 12 Union Road, Cambridge CB2 1EZ, U.K., fax +44 1223 336033.

# 2.3. Neutron powder diffraction (NPD)

Time-of-flight neutron powder diffraction (ToF-NPD) data were acquired at the Spallation Neutron Source at Oak Ridge National Laboratory on the high-resolution neutron powder diffractometer POWGEN. Two samples, one germanide and one stannide, each approximately 2.5 g, were loaded in vanadium cans (8 mm inner diameter), which were sealed with brass gaskets. The high-resolution datasets were collected at 100 K, covering a *d*-spacing range from 0.5 to 7 Å. The Rietveld refinements were performed using GSAS-II. <sup>56</sup> Atomic coordinates and labels were set to be consistent with the SCXRD data. During the Rietveld refinements the scale factor, two profile shape parameters, lattice parameters, fractional coordinates of the atoms, and their displacement parameters were optimized. We note that the TOF profile function for POWGEN varies from the standard line shape originally derived for GSAS. <sup>57</sup>

#### 2.4. Synchrotron X-ray powder diffraction (SXPD)

The small portions of the prepared powder samples for NPD were set aside, and later used for SXPD.

As stated above, all work was done inside the glovebox and the powders were loaded in Kapton

capillaries with 0.8 mm inner diameter, which were sealed by using wax. The high-resolution synchrotron powder diffraction data were collected at the Brockhouse High Energy Wiggler beamline of the Canadian Light Source, Canada using 35.45 keV (0.3497 Å) X-ray and a Varex XRD 4343 CT detector. The data processing and the Rietveld refinements were carried out using the GSAS-II software.<sup>56</sup>

# 2.5. Electronic structure calculations

The electronic band structures were calculated using the Stuttgart TB-LMTO-ASA code with the local density approximation (LDA) exchange-correlation functional.  $^{58,59}$  The von Barth-Hedin type of the LDA functional was employed. To satisfy the atomic sphere approximation (ASA), empty spheres were introduced where needed.  $^{60}$  The Brillouin zones were sampled with a k-point step of about 0.1 Å $^{-1}$ . Chemical bonding was interrogated using the Crystal Orbital Hamilton Population (COHP) approach and Electron Localization Function (ELF).  $^{61}$  Integrations of electron density were performed with the program Critic2.  $^{62}$ 

### 3. RESULTS AND DISCUSSION

# 3.1 Notes on the synthesis

As noted earlier, there exist some controversies surrounding lithium germanide binaries, both from an experimental standpoint and from a point of view of computationally predicted <sup>40,47</sup> phases that lack experimental validation. To this end, we tried to (re)synthesize several phases with different Li/Ge ratio, as such: Li<sub>3</sub>Ge<sub>2</sub> (Li/Ge = 1.5), Li<sub>11</sub>Ge<sub>6</sub> (Li/Ge = 1.83), Li<sub>2</sub>Ge (Li/Ge = 2), Li<sub>9</sub>Ge<sub>4</sub> (Li/Ge = 2.25), Li<sub>7</sub>Ge<sub>3</sub> (Li/Ge = 2.34), Li<sub>13</sub>Ge<sub>5</sub> (Li/Ge = 2.4), Li<sub>8</sub>Ge<sub>3</sub> (Li/Ge = 2.67), Li<sub>11</sub>Ge<sub>4</sub> (Li/Ge = 2.75), Li<sub>3</sub>Ge (Li/Ge = 3), Li<sub>13</sub>Ge<sub>4</sub> (Li/Ge = 3.25) and Li<sub>7</sub>Ge<sub>2</sub> (Li/Ge = 3.5). In most cases, after examining the products from each synthesis by PXRD, there appeared to be only peaks from reported phases (Table S1). For example, the

reaction products of the "Li<sub>13</sub>Ge<sub>5</sub>" reaction were Li<sub>5</sub>Ge<sub>2</sub> and Li<sub>7</sub>Ge<sub>2</sub> (N.B. Li<sub>5</sub>Ge<sub>2</sub> and Li<sub>7</sub>Ge<sub>2</sub> are the formulae from the records in the crystallographic database, the actual chemical formulae are Li<sub>5-x</sub>Ge<sub>2</sub> and Li<sub>7-x</sub>Ge<sub>2</sub>, as discussed later in this paper). The major product of the "Li<sub>7</sub>Ge<sub>3</sub>" reaction was also the rhombohedral Li<sub>5</sub>Ge<sub>2</sub> phase.<sup>30</sup> This is not unexpected since Li<sub>7</sub>Ge<sub>3</sub> (Li/Ge = 2.33) and Li<sub>5</sub>Ge<sub>2</sub> (Li/Ge = 2.5) are compositionally very close.

Single-crystal X-ray diffraction work was simultaneously commenced to validate the crystal structures, particularly those that had been reported without displacement parameters and/or with high residuals. Working with several crystals from what appeared to be a recurring phase in many syntheses, Li<sub>3</sub>Ge<sub>2</sub>, it became obvious that Li<sub>5</sub>Ge<sub>2</sub> is a phase with a small homogeneity range. The results from four different refinements for a single-crystal selected from the "7-3" batch are summarized in Table 1; they are a testament to the difficulties that can be encountered/expected when discerning the best structural model in similar situations.

Table 1. Selected crystallographic data for Li<sub>5</sub>Ge<sub>2</sub> (Mo  $K\alpha$ ,  $\lambda$  = 0.71073 Å; Space group  $R\overline{3}m$ , no. 166; Z = 3). The same data set is refined against four different models—model **I** is with all atoms being fully occupied; model **II** is with all atoms being fully occupied and Li and Ge mixed (ca. 99:1(1) ratio) at the Li site which is showing occupation factor greater than 1; model **III** is with all atoms being fully occupied, except for the Li atom on special position 0, 0, 0, which had a refined occupation factor 0.63(5); model **IV** is composed by model **II** and model **III** taken together. CCDC code for the latter is 2340451.

	Model	I	II	III	IV
•	Chemical formula	Li <sub>5</sub> Ge <sub>2</sub>	Li <sub>4.98(1)</sub> Ge <sub>2.02</sub>	Li <sub>4.7(1)</sub> Ge <sub>2</sub>	Li <sub>4.7(1)</sub> Ge <sub>2.02(1)</sub>
	fw/ g mol <sup>-1</sup>	179.88	180.97	177.57	179.01

a/ Å	4.4605(3)	4.4605(3)	4.4605(3)	4.4605(3)
c/ Å	18.3243(17)	18.3243(17)	18.3243(17)	18.3243(17)
V/ Å <sup>3</sup>	315.74(4)	315.74(4)	315.74(4)	315.74(4)
$Q_{\rm calc}$ / g cm <sup>-3</sup>	2.84	2.86	2.80	2.83
$\mu(\text{Mo }K\alpha)/\text{ cm}^{-1}$	140.4	141.5	140.3	141.5
$R_1 (I > 2\sigma_{(I)})^a$	0.0158	0.0155	0.0143	0.0143
$wR_2 (I > 2\sigma_{(I)})^a$	0.0363	0.0341	0.0310	0.0304
$R_1$ (all data) <sup>a</sup>	0.0182	0.0178	0.0165	0.0165
$wR_2$ (all data) <sup>a</sup>	0.0369	0.0347	0.0316	0.0308
$\Delta \varrho_{\rm max;min}/ {\rm e}^{-}\dot{\rm A}^{-3}$	0.47; -0.46	0.46; -0.45	0.45; -0.45	0.45; -0.43

a  $R_1 = \sum ||F_o| - |F_c|| / \sum |F_o|$ ;  $wR_2 = [\sum [w(F_o^2 - F_c^2)^2] / \sum [w(F_o^2)^2]]^{1/2}$ , where  $w = 1/[\sigma^2 F_o^2 + (AP)^2 + (BP)]$  and  $P = (F_o^2 + 2F_c^2) / 3$ . A and B are the respective weight coefficients (see the CIF data).

The last point of discussion with regards to the synthesis concerns the possibility of an inadvertent crucible material reaction with the Li-Ge melts. It is recognized that Nb containers may react with Ge, in particular, <sup>63</sup> producing Nb-contaminated samples. To rule out "crucible effects", reactions were also carried out in sealed Ta containers at the same temperature conditions. The refinements of the structure for such crystals were indistinguishable from those obtained from experiments in Nb tubes, indicating that the grown crystals are devoid of Nb.

# 3.2. Notes on single-crystal X-ray diffraction

As evidenced from Table 1, four structural models were tried when fitting the intensity data from single-crystal X-ray diffraction experiments. In one, Li and Ge are mixed-occupied (ca. 99:1(1) ratio) at the Li site showing occupation factor greater than 1 (vide infra). In another one, the Li atom on special

position 3a (at the origin), which had a refined occupation factor 0.63(5), was considered with fractional occupancy, leading to the conjecture that the phase is off-stoichiometric with respect to Li. In this regard, we caution that refining the occupancies of such light elements like Li, from X-ray diffraction data alone, is not an ideal method for ascertaining Li-occupational disorder, even though the displacement parameter value of the lithium atom at site 3a decreased noticeably when its occupancy was refined (for a multitude of crystals from different synthetic batches). Importantly, neutron powder diffraction also indicated improved refinement when the occupancy parameter of this site was freed. Taken altogether, the results from the refinements show apparent Li deficiency, both from SCXRD and NPD data, with final refined composition Li<sub>4.7(1)</sub>Ge<sub>2</sub>. It is worthwhile mentioning here that almost the same amount of Li defects has been reported by von Schnering et al. with regards to Li<sub>4.67</sub>Si<sub>2</sub>.<sup>48</sup> On this note, we also draw attention to the fact that 1/3 vacancies, particularly in a rhombohedral structure, can be an indicator for the possible existence of a superstructure with ordered defects - ordering can manifests itself in another rhombohedral strtucture with altered stacking sequence, or in a reduced symmetry, such as Li<sub>7</sub>Ge<sub>3</sub> in the trigonal space group P3<sub>1</sub>21, predicted by Morris et al.<sup>47</sup> To date, we have not found an experimental evidence for that. We also disclose that even though there is a slight improvement of the conventional residuals when Li/Ge mixing was considered (Table 1, model IV), no statistically significant effect could be inferred from the refinements.

To better understand the phase behavior and to help us model the disorder present in this structure, we followed up with several more experiments with nominal compositions  $\text{Li}_{5-x}\text{Ge}_{2+x}$ , where x values increase in increments of 0.1 from x=0 to x=0.5. A crystalline rhombohedral phase was the product up to x=0.2, with single-crystal refinements giving very similar results—there are barely distinct differences between the refined compositions, yet, judging from the variations in the Ge–Ge distances and the small improvement of the refinement statistics upon introducing of disorder, they are not stoichimetric  $\text{Li}_5\text{Ge}_2$  (Table 2).

Table 2. Selected crystallographic data for three more independent  $\text{Li}_{5-x}\text{Ge}_2$  samples (Mo  $K\alpha$ ,  $\lambda = 0.71073$  Å; Space group  $R\ \bar{3}m$ , no. 166; Z=3). Residual values indicated in brackets are from the refinements where partial Li-occupancy for the Li atom on special position  $3a\ (0,0,0)$  was not considered. All atoms were refined with anisotropic displacement parameters, including Li.

Chemical formula	$Li_{4.7(1)}Ge_2$	$Li_{4.7(1)}Ge_2$	$Li_{4.7(1)}Ge_2$
fw/ g mol <sup>-1</sup>	177.80	177.80	177.80
a/ Å	4.4674(6)	4.4674(5)	4.4634(4)
c/ Å	18.328(3)	18.324(3)	18.323(3)
<i>V</i> / Å <sup>3</sup>	316.78(8)	316.71(7)	316.12(6)
$Q_{\rm calc}$ / g cm <sup>-3</sup>	2.80	2.80	2.80
$\mu({ m Mo}~Klpha)/~{ m cm}^{-1}$	140.0	140.0	140.0
$R_1 (I > 2\sigma_{(I)})^a$	0.0200 {0.0213}	0.0168 {0.0177}	0.0176 {0.0189}
$wR_2 (I > 2\sigma_{(I)})^a$	0.0418 {0.0474}	0.0344 {0.0356}	0.0346 {0.0403}
$R_1$ (all data) <sup>a</sup>	0.0241 {0.0248}	0.0219 {0.0225}	0.0202 {0.0214}
$wR_2$ (all data) <sup>a</sup>	0.0428 {0.0485}	0.0348 {0.0368}	0.0353 {0.0409}
$\Delta Q_{\text{max;min}} / e^- \cdot \text{Å}^{-3}$	0.87; -0.44	0.86; -0.82	0.61; -0.58
CCDC code	2340452	2340453	2340454

<sup>&</sup>lt;sup>a</sup>  $R_1 = \sum ||F_o| - |F_c|| / \sum |F_o|$ ;  $wR_2 = [\sum [w(F_o^2 - F_c^2)^2] / \sum [w(F_o^2)^2]]^{1/2}$ , where  $w = 1 / [\sigma^2 F_o^2 + (AP)^2 + (BP)]$  and  $P = (F_o^2 + 2F_c^2) / 3$ . A and B are the respective weight coefficients (see the CIF data).

For samples with nominal compositions  $\text{Li}_{5+/-x}\text{Ge}_2$ , where x > 0.3, the crystallinity was poor and suitable crystals to measure on the diffractometer could not be obtained. By PXRD, the samples were multi-phase mixtures. This indicates that crystallization of the rhombohedral  $\text{Li}_5\text{Ge}_2$  phase is favored in Li/Ge ratios from ~2.6 to ~2.2, with the optimal being ~ 2.4, i.e., the actual chemical formula of this compound should be considered as  $\text{Li}_{5-x}\text{Ge}_2$  ( $x \approx 0.3$ ).  $\text{Li}_7\text{Ge}_3$ , the computationally predicted <sup>47</sup> trigonal phase that was

targeted can also be expressed as Li<sub>4.67</sub>Ge<sub>2</sub>, which may indicate the ground state structure for this composition is indeed the Li-defect Li<sub>5-x</sub>Ge<sub>2</sub> version of the rhombohedral "5:2" phase.

At this point, with the hypothesis for off-stoichiometry in the germanide confirmed, we decided to take a closer look at the Li-Sn system, where the crystal structure of  $\text{Li}_5\text{Sn}_2$  had been known for many years (although atomic displacement parameters had not been reported in the 1975 paper).<sup>34</sup> Not surprisingly, slightly different non-stoichiometric behavior was quickly discovered. Since Sn is heavier than Ge (and much heavier than Li), the refinements from SCXRD data of three independent crystals (Table 3) clearly indicated that on one Li site, Li1, the occupation factor was 2-3 times greater than 1. In the absence of evidence for a another element in the sample, the model employed for the final refinements had Li and Sn atoms randomly distributed (up to ca. 88:12(1) ratio). We also note that rhombohedral  $\text{Li}_{5-x}\text{Sn}_{2+x}$  phase only forms in a nicely crystalline form when x value does not approach/exceed 0.1. When  $x \ge 0.1$ , the reactions yield monoclinic  $\text{Li}_7\text{Sn}_3$  instead. Given the very close compositions, that is not unexpected.

Table 3. Selected crystallographic data for three independent  $\text{Li}_{5-x}\text{Sn}_{2+x}$  crystals (Mo  $K\alpha$ ,  $\lambda=0.71073$  Å; Space group  $R\,\overline{3}m$ , no. 166; Z=3). All atoms were refined with anisotropic displacement parameters, including Li.

Chemical formula	$\text{Li}_{4.96(2)}\text{Sn}_{2.04}$	$\text{Li}_{4.92(1)}\text{Sn}_{2.08}$	$\text{Li}_{4.82(1)}\text{Sn}_{2.18}$
fw/ g mol <sup>-1</sup>	276.55	281.02	292.20
a/ Å	4.7271(10)	4.7203(9)	4.717(3)
c/ Å	19.727(7)	19.737(5)	19.78(2)
<i>V</i> / Å <sup>3</sup>	381.76(17)	380.85(14)	381.2(6)
$Q_{\rm calc.}/{\rm g~cm^{-3}}$	3.61	3.68	3.82
$\mu(\text{Mo }K\alpha)/\text{ cm}^{-1}$	98.0	100.7	104.9
$R_1 (I > 2\sigma_{(I)})^{a}$	0.0375	0.0119	0.0202

$wR_2 (I > 2\sigma_{(I)})^{a}$	0.0731	0.0263	0.0466
$R_1$ (all data) <sup>a</sup>	0.0445	0.0129	0.0217
$wR_2$ (all data) <sup>a</sup>	0.0749	0.0267	0.0469
$\Delta Q_{\text{max;min}} / e^{-} \cdot \mathring{A}^{-3}$	1.37; -1.23	0.51; -0.58	0.90; -1.18
CCDC code	2340455	2340456	2340457

<sup>&</sup>lt;sup>a</sup>  $R_1 = \sum ||F_o| - |F_c|| / \sum |F_o|$ ;  $wR_2 = [\sum [w(F_o^2 - F_c^2)^2] / \sum [w(F_o^2)^2]]^{1/2}$ , where  $w = 1/[\sigma^2 F_o^2 + (AP)^2 + (BP)]$  and  $P = (F_o^2 + 2F_c^2) / 3$ . A and B are the respective weight coefficients (see the CIF data).

# 3.3. Notes on synchrotron and neutron diffraction data

As noted in the previous section, there are clear variations in the lattice parameters obtained from SCXRD (Tables 2 and 3). The same differences can be discerned by a quick visual inspection of the experimental powder patterns (Figure S1 and S2). For instance, one can see the shift of highest intensity peak on the NPD and synchrotron XRD pattern from that of simulated XRD pattern at d-value of ca. 4 Å for the  $Li_{5-x}Sn_{2+x}$  phase (Figure S1); shifts of highest intensity peak at d-value of 3.8 Å or the peak at higher d-value of about 6.1 Å are also noticeable for the germanide (Figure S2). This is evidence related to the change in unit cell volume in response to the change in the synthetic conditions, signaling that the bulk samples also do not have a fixed composition.

Due to the higher Z-contrast between Li and Sn, both single-crystal and powder X-ray diffraction methods allow for a relatively straightforward interpretation of the probable Li/Sn disorder in Li<sub>5-x</sub>Sn<sub>2+x</sub>. Powder neutron diffraction work helped confirm that line of thought. Specifically, joint Rietveld refinements of the occupancy factor of the Sn atom also give no deviations from 100% for all three datasets (Figure 1), while refinements of the site occupancy factor (SOF) of the lithium atoms resulted in unphysical values approaching 200% for the Li1 atom in all datasets. For comparison, the occupancy factors for Li2 and Li3 fluctuated between 87% and 107% with no trend and most importantly with very

large estimated standard deviations (e.s.d.). Introducing the statistical admixing of Li and Sn at 6c site (Li1 atom) led to much improved R-value. The Rietveld refinements of SXPD and NPD data for  $\text{Li}_{5-x}\text{Sn}_{2+x}$  are complicated due to the few small peaks from an impurity phase. It is difficult to trace the origin of them, since for preparing the powder samples, we did several sealed-tube experiments containing 0.5 g of each sample. Later, samples from each batch were ground using mortar and pestle in the glove box to get sufficient amount to carry out the powder diffraction experiments.

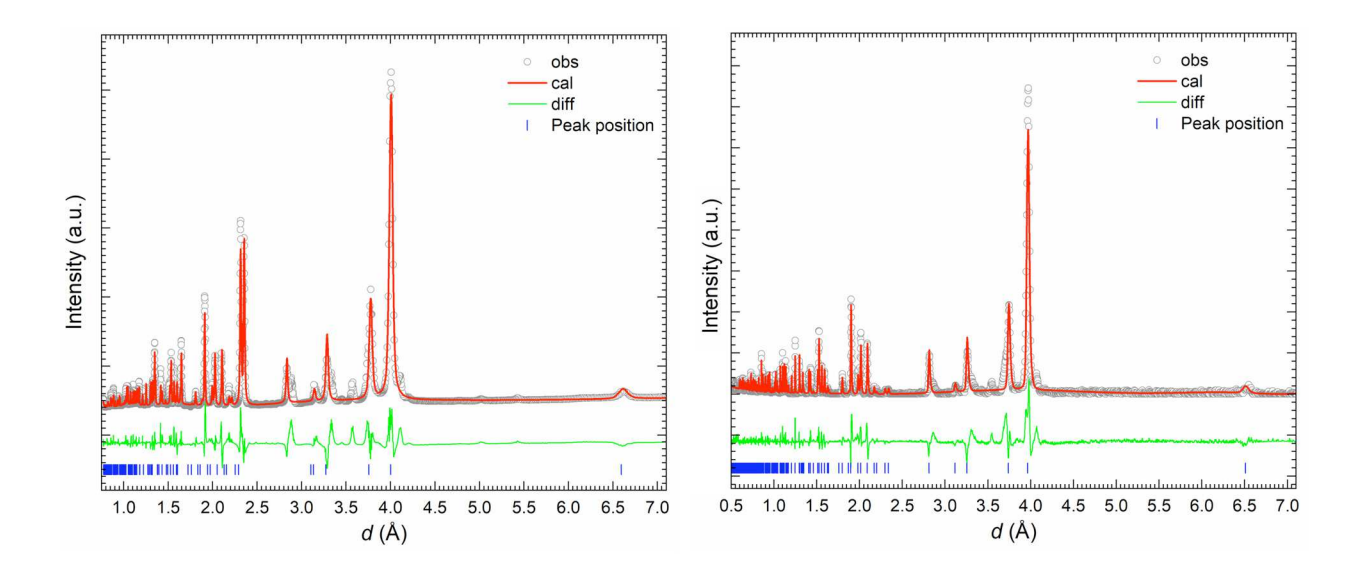


Figure 1. Rietveld refinement plots of synchrotron powder X-ray diffraction data (left), and neutron powder diffraction data (right) for  $\text{Li}_{5-x}\text{Sn}_{2+x}$ . Few weaker peaks remain unidentified, indicating presence of small amount of impurity. The refined atomic coordinates and isotopic displacement parameter are tabulated in Table S2 and S3, respectively.

Structural disorder in the "5-2" lithium germanide is more subtle, as already deduced from refinements of SCXRD data (Table 1 and 2). Although we do see variations in the unit cell parameters from sample to sample, the data for the bulk are not presenting an unambiguous picture (Figure 2). Specifically: i)

Refinements of the SOF of the Li atoms here give no significant deviations above 100%. The largest unphysical (more than 100%) values were 110-125%, and the e.s.d.'s were large, barely above the  $3\sigma$ threshold; ii) The "heavy" Li atom here was Li2, while in Li<sub>5-x</sub>Sn<sub>2+x</sub>, the offending site was Li1; iii) Displacement parameter of lithium atom Li3 at site 3a was noticeably larger compared to the other two Li atoms. Freeing the SOF of Li3 resulted in SOF of about 70% and much improved  $U_{\rm iso}$  value (based on NPD data). The conventional residuals also dropped, suggestive of an overall improved fit of the intensity data to the structural model. Rietveld refinements parameters (Table S2 and Table S3) are in very good agreement with the SCXRD refinements. One may notice the higher displacement parameter for Li3. Since this atom is on a special position, it is hard to conclude if positional disorder is the culprit. That can be possibly resolved by temperature dependent diffraction studies, which was not a goal for this study. At this stage, one could also consider the possibility of concurrent defects and substitutional disorder—a parallel could be drawn between the structure under consideration and the structure of the type-I clathrate  $K_8 \text{Li}_x \text{Ge}_{44-x/4} \square_{2-3x/4} \ (0 < x < 2.67; \ \square \ \text{denotes vacancy}).^{64,65} \ \text{If this was the case here, then the actual formula}$ can be denoted as  $\text{Li}_{5-x}\Box_y\text{Ge}_{2+x+y}$ , where x and y are two independent variables. In the work studying the  $K_8Li_xGe_{44-x/4}\square_{2-3x/4}$ , Liang et al. showed gradual incorporation of Li atoms into the 6c site of the Ge framework, which indicates that the Li and vacant Ge atoms could be considered together on that particular crystallographic site. 65 Under those circumstances, the particular elongation of the displacemnt ellipsoids of the Ge atoms becomes highly informative. From the structural data available at present, we see nothing unusual with regards to  $U_{ij}$  elements, and therefore, can argue that it is impossible to conclude the presence of other vacancies in the structure, besides those already discussed at the Li3 special position.

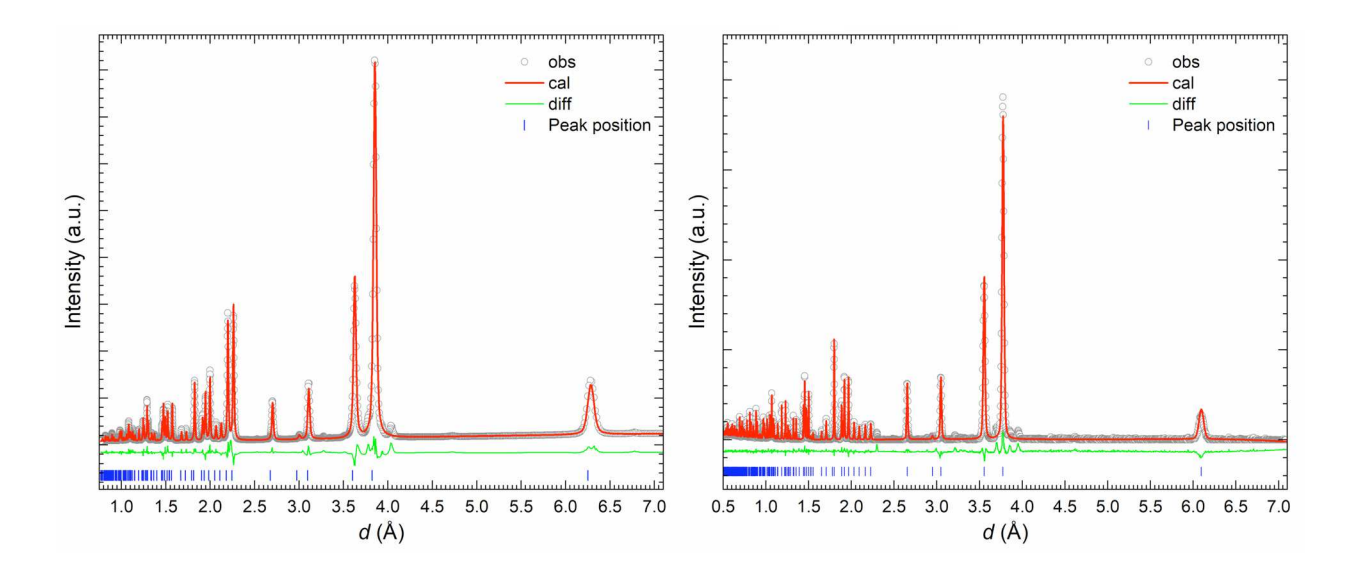


Figure 2. Rietveld refinement plots of synchrotron powder X-ray diffraction data (left), and neutron powder diffraction data (right) for Li<sub>5-x</sub>Ge<sub>2</sub>.

To sum up this discussion we note that a similar structure with Li defects already has a precedent—von Schnering *et al.* studied the isotypic silicide Li<sub>2,33</sub>Si,<sup>48</sup> (this corresponds to Li<sub>4,67</sub>Si<sub>2</sub>, i.e. Li<sub>5-x</sub>Si<sub>2</sub> (x = 0.33)), whose structural intricacies and disorder mirror those of the model that yielded the refined composition Li<sub>-4,7</sub>Ge<sub>2</sub>. Coincidently, Li<sub>-4,7</sub>Ge<sub>2</sub>  $\approx$  Li<sub>7</sub>Ge<sub>3</sub>, the lithium germanide "7:3" phase that had been computationally predicted not too long ago, and speculated to crystallize in trigonal syngony with the space group  $P3_121$ )<sup>47</sup>. We will recall that Li<sub>7</sub>Ge<sub>3</sub> was what we aimed to experimentally validate in a first place, since based on delithiation work, Grey *et. al.* had suggested that latter phase is thermodynamically more stable than Li<sub>5</sub>Ge<sub>2</sub> (which is viewed as another, intermediate phase).<sup>66</sup> Considering the presence of vacant lithium atoms in Li<sub>3</sub>Ge<sub>2</sub>, which results in the chemical formula Li<sub>-4,7</sub>Ge<sub>2</sub>, it is possible, that the computations that predict stability for Li<sub>7</sub>Ge<sub>3</sub> capture a local order in the otherwise globally disordered Li<sub>5-x</sub>Ge<sub>2</sub> phase. If crystallographic ordering were to happen on a longer range, then the 6 times larger unit cell volume and lower symmetry could allow the rest of the structure to "relax" around the defects. However, we are unable to see experimental evidence that such ordered structure exists as predicted.

# 3.4. Crystal structure and structural relationships

Notwithstanding the disorder described above, the crystal structure is simple, and it is assigned to the  $\text{Li}_5\text{Tl}_2$  type (space group  $R\ \bar{3}m$ , no. 166; Z=3; Pearson symbol hR7). There are four crystallographically unique positions in the asymmetric unit (Figure 3), including one tin or germanium atom (at site 6c) and three lithium atoms (two at sites 6c and another at site 3a).

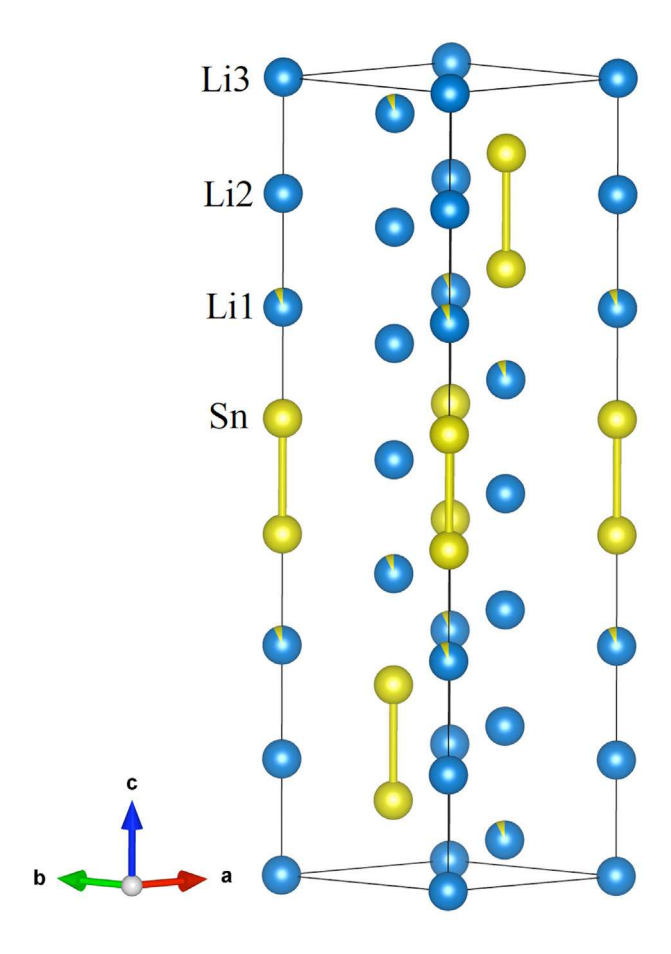


Figure 3. Schematic representation of the rhombohedral crystal structure of  $\text{Li}_{5-x}\text{Sn}_{2+x}$ . Blue and yellow colors represent the lithium and tin atoms, respectively. The Li/Sn disorder is shown with partial shading of the Li1 atom at 6c site. For  $\text{Li}_{5-x}\text{Ge}_2$ , such Li/Ge disorder cannot be discerned, but there are approx.

30% defects on the Li special position 0, 0, 0 (at the origin). The average distances within the dumbbells are:  $d_{\text{Ge-Ge}} = 2.50 \text{ Å}$ ;  $d_{\text{Sn-Sn}} = 2.86 \text{ Å}$ .

Below we will use the structure of  $\text{Li}_{-4.7}\text{Ge}_2$  to start the discussion, since the variations from the ideal "5-2" structure here are less significant compared to the structure of  $\text{Li}_{5-8}\text{Sn}_{2+x}$ . The structure contains Ge–Ge dimers that are enclosed in a cage of 20 lithium atoms, as shown in Figure 4a. Six Li2 atoms arrange themselves in a puckered six-membered ring that wraps around the dumbbell. Four Li1 and three Li3 atoms coordinate the Ge atoms on the top and bottom. The Ge–Li distances vary in a wide range, between 2.58 Å and 3.15 Å. Li–Li distances also fall in wide range, with some as short as 2.67 Å. The Ge–Ge distances vary from sample to sample (2.4883(9) Å to 2.502(1) Å), which is another evidence to support the hypothesis that valence electron count is varied as a result of small changes in the Li3-occupancy. Additional details concerning  $d_{\text{Ge-Ge}}$  will be discussed later on. A view of the extended array of Ge<sub>2</sub> dumbbells is depicted in Figure 4b. A very similar environment can be seen in the structure of Li<sub>3</sub>NaGe<sub>2</sub>, where Ge–Ge dimers are coordinated by a total of 15 alkali atoms (11 Li and 4 Na atoms). Notably, the Ge is less-reduced in Li<sub>3</sub>NaGe<sub>2</sub>, and therefore, the Ge–Ge distances are much shorter, 2.390(1), Å which was concluded to be a signature of a Ge=Ge double bond.<sup>67</sup>

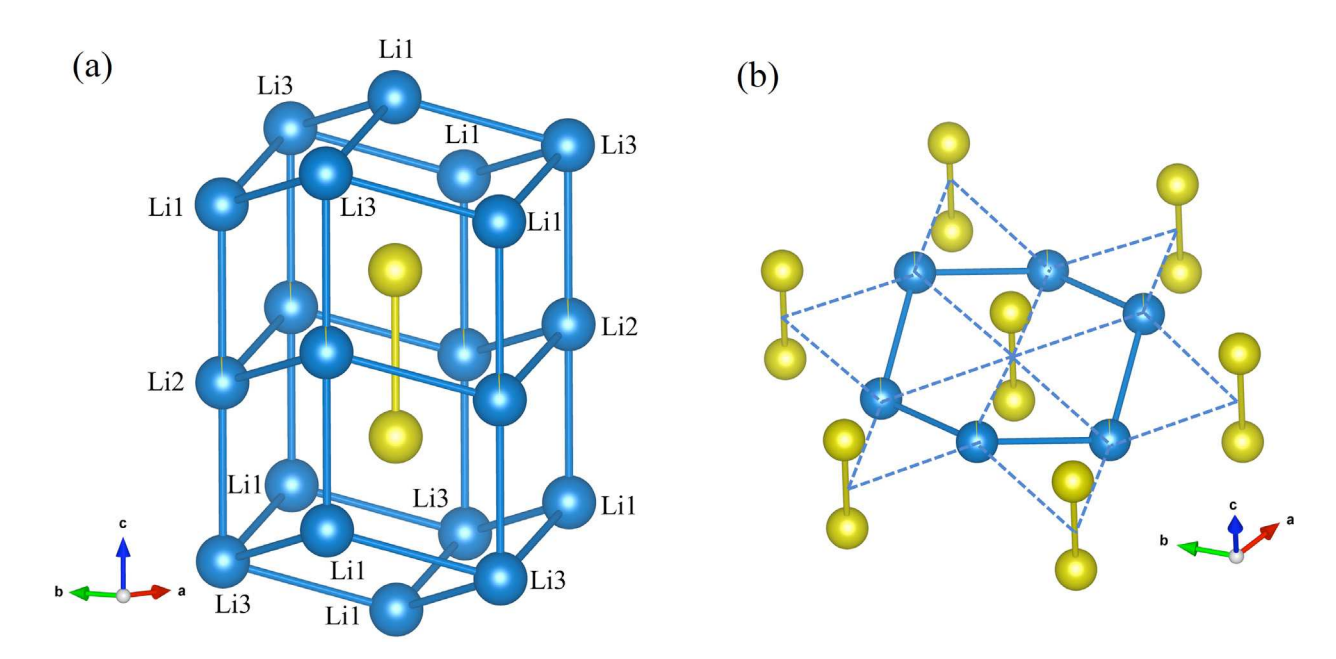


Figure 4. (a) The  $Ge_2$  dumbbell, enclosed by an average of 20 Li atoms. Notice that there are six Li3 atoms in the drawing, and considering the 2/3 occupation factor for Li3, a more accurate way to describe the polyhedron is as being made of 18 Li atoms in total. (b) An extended view of the local environment of  $Ge_2$  dumbbells.

Another way to view the crystal structure is to consider it as a stacking sequence of corrugated Li layers that make a distorted hexagonal packing in the *c*-direction; Ge-atoms are situated between the layers as shown in Figure 5a. One should notice that there are two types (Figure S3) of puckered hexagonal sheets of Li atoms—one with Li atoms residing in the middle of the six-membered ring and another where the electron density at the center of the ring is contributed by the electrons localized between the Ge atoms situated above and below. This arrangement bears some similarity with the structure of the quaternary phase BaIn<sub>2</sub>Li<sub>2</sub>Ge<sub>2</sub>,<sup>68</sup> which also crystallizes in same rhombohedral space group. In the latter structure, In<sub>2</sub>Ge<sub>6</sub> double-layers with lithium atoms residing within them are found, as shown in Figure 5b, and they also form puckered hexagonal sheets. In this case, the six-membered ring "halves" the In–In dumbbell. The much larger Ba atoms are located in the space between adjacent slabs. The arrangement of the Ge

atoms also builds up a distorted hexagonal close packing making a honeycomb-like structure (Figure 5c), while lithium atoms in  $\text{Li}_5\text{Ge}_2$  resemble the distorted hexagonal packing when viewed in the projection of the c-axis.

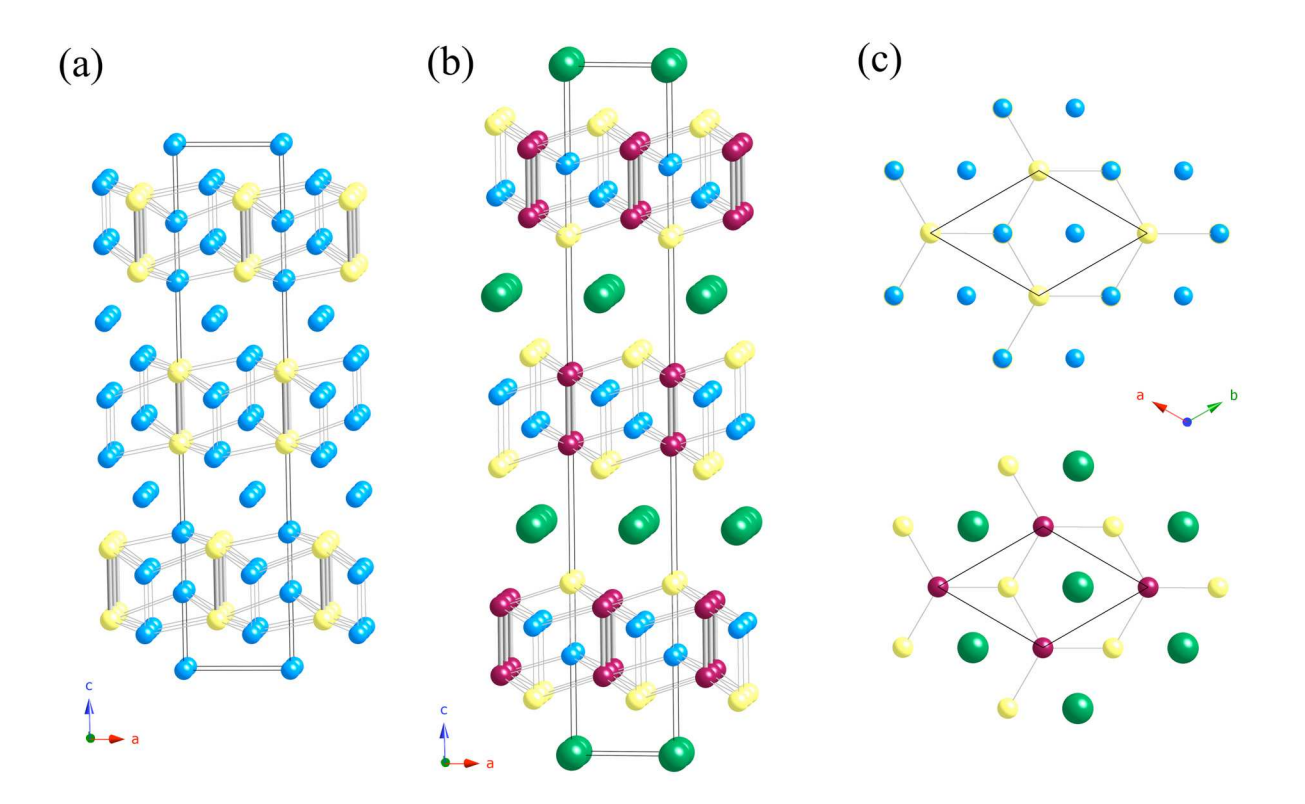


Figure 5. (a) Structure of idealized  $\text{Li}_5\text{Ge}_2$ , viewed as slabs of tetrahedrally coordinated Li (light blue), where Ge atoms (yellow) are situated. Octahedrally coordinated Li atoms are found between these slabs and shown without bonds drawn. (b) Structure of  $\text{BaLi}_2\text{In}_2\text{Ge}_2$ , also viewed as slabs of tetrahedrally coordinated Li (light blue). Ge atoms (yellow) and In atoms (maroon) form corrugated layers. Octahedrally coordinated Ba atoms (green) are found between these slabs and shown without bonds drawn.. (c) Top views of layer fragments of both structures centered ar z = 1/3. As it may be obvious from the schematic representations in this figure, rhombohedral  $\text{BaLi}_2\text{In}_2\text{Ge}_2$  and  $\text{Li}_5\text{Ge}_2$  are isotypic (Pearson symbol hR7, Wyckoff  $b^3a$ ). A different representation (Figure S4) shows  $\text{BaLi}_2\text{In}_2\text{Ge}_2$  as a "colored" variant of  $\text{Li}_5\text{Ge}_2$ .

The Ge–Ge moieties are common structural motifs in several other Li-Ge phases.<sup>21,22</sup> For example, dumbbells are also found in the structure of Li<sub>9</sub>Ge<sub>4</sub>, which has been reported to crystallize in the orthorhombic crystal system with space group *Cmcm* (No. 63). The structural identification was done in 1970.<sup>21</sup> Another relevant structure is that of Li<sub>7</sub>Ge<sub>2</sub>, which crystallizes in an orthorhombic crystal system with space group *Cmmm* (No. 65), reported in 1972. Without going into the specifics, we want to mention that both crystal structures are currently being reassessed, and that the full crystallographic details will be presented in a future article.

Considering that the refined Ge-Ge (2.50 Å) and Sn-Sn (2.86 Å) distances are close to the sum of the respective covalent radii ( $r_{\rm Ge}=1.22$  Å,  $r_{\rm Sn}=1.44$  Å), <sup>69</sup> some discussion along the lines of the Zintl concept can be instructive. Of particular interest are the distance variations as they pertain to deviations from the ideas of 2-center 2-electron bonding within the Sn-Sn or Ge-Ge dumbbells (Figure 6). For example, in the structure of Li<sub>9</sub>Ge<sub>4</sub> (normalized to 1 equivalent Ge, it can be rewritten as Li<sub>2.25</sub>Ge), the Ge-Ge dumbbells show  $d_{\text{Ge-Ge}}$  of 2.44 Å.<sup>21</sup> Upon further reduction by virtue of increasing the Li content, as in the  $Li_{5-x}Ge_2$  structure (for  $x \approx 0.3$ , the formula can be rewritten as  $Li_{-2.35}Ge$  when normalized to 1 equivalent Ge), the Ge-Ge bond length increases. One should note that the refined  $d_{\text{Ge-Ge}}$  for several independent samples vary from 2.4883(9) Å to 2.502(1) Å, indicative of the varied valence electron count. The structure of the lithium richer  $\text{Li}_{7-x}\text{Ge}_2$  ( $x \approx 0.5$ ) consists of Ge–Ge dumbbells with isolated Ge atoms (Figure 6c). With the Ge atom being even more reduced here, it is not surprising that the  $d_{\text{Ge-Ge}}$  is the longest (~2.62 Å).<sup>22</sup> This progression was also noted in the publication by Grey et. al. in which the in situ lithiation of Ge anodes was reported to involve gradual increasing of  $d_{Ge-Ge}$ , which ultimately leads to breakage of Ge-Ge bonds. 66 The suggested therein pathway Li<sub>9</sub>Ge<sub>4</sub> (Li<sub>2.25</sub>Ge) → Li<sub>7</sub>Ge<sub>3</sub> (Li<sub>2.33</sub>Ge) →  $\text{Li}_7\text{Ge}_2$  ( $\text{Li}_{3.5}\text{Ge}$ )  $\rightarrow$   $\text{Li}_{15}\text{Ge}_4$  ( $\text{Li}_{3.75}\text{Ge}$ , with no Ge–Ge dumbbells) is in line with the previous discussion. The crystal structures of the Li<sub>0</sub>Ge<sub>4</sub> and Li<sub>7</sub>Ge<sub>2</sub> phases, as mentioned already, are currently being reassessed by us. At least for the latter, from the structural data in hand, we can affirmatively state that  $\text{Li}_7\text{Ge}_2$  should be considered as  $\text{Li}_{7-x}\text{Ge}_2$  ( $x\approx 0.5$ ), mirroring the Li-deficiency in  $\text{Li}_{7-x}\text{Si}_2$  ( $x\approx 0.5$ ), which has also been denoted as  $\text{Li}_{13}\text{Si}_4$ .

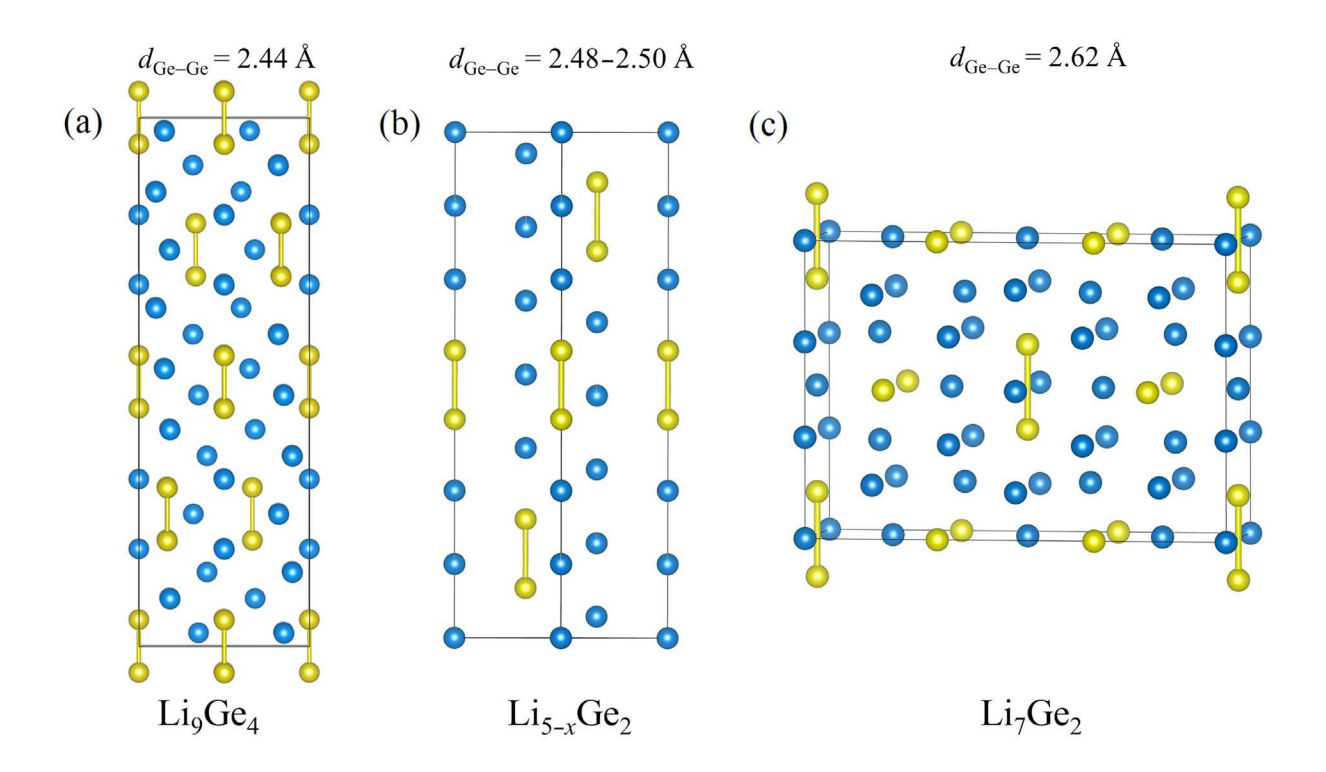


Figure 6: Schematic representations of the crystal structures of (a) Li<sub>9</sub>Ge<sub>4</sub> (ICSD#25308),<sup>20</sup> (b) Li<sub>5-x</sub>Ge<sub>2</sub> (*this work*) and (c) Li<sub>7</sub>Ge<sub>2</sub> (ICSD#42063).<sup>21</sup> The blue and yellow colors represent lithium and germanium atoms, respectively. The Ge–Ge dumbbells are indicated by the yellow cylinders and the respective distances are marked.

The discussion above can be generalized following the Zintl concept. Assuming 2-center 2-electron interaction within the Ge–Ge dumbbells, the following schemes for partitioning of the valence electrons in the above mentioned compounds can be proposed:

$$\text{Li}_7\text{Ge}_2 = \text{Li}_{14}\text{Ge}_4 = (\text{Li}^+)_{14}(\text{Ge}_2^{6-})(\text{Ge}^{4-})_2$$

$$Li_{5-x}Ge_2 = (Li^+)_{4.7}(Ge_2^{4.7-}) \{ for \ x \approx 0.3 \}$$

$$\text{Li}_{9}\text{Ge}_{4} = 2\times[(\text{Li}^{+})_{4.5}(\text{Ge}_{2})^{4.5-})]$$

As mentioned above, the expectation that as Li content increases, Ge becomes more reduced and bond order diminishes is followed. In Li<sub>9</sub>Ge<sub>4</sub>, based on the electron count and the shortest distance between Ge atoms (Figure 6), the bond order should be close to 2, i.e.,  $[Ge=Ge]^4$ , notwhistanding the excess of 0.5 electron per dimer. A true precedent for  $[Ge=Ge]^4$  does exist, as noted earlier, in the closely related Li<sub>3</sub>NaGe<sub>2</sub>,<sup>67</sup> where  $d_{Ge-Ge}$  is even shorter than 2.4 Å. The other extreme is in Li<sub>7</sub>Ge<sub>2</sub>, where the bond order should be considered to be 1, i.e.  $[Ge-Ge]^{6-}$ , corresponding to a significantly longer distance of approx. 2.6 Å. The case of Li<sub>5-x</sub>Ge<sub>2</sub> is clearly in between the "end" members. Another example of intermediate bond order and intricate contribution of Li to  $\pi$ -bonding concerning Ge–Ge bonds is the structure of Ba<sub>2</sub>LiGe<sub>3</sub>, or rather Ba<sub>2</sub>Li<sub>1-x</sub>Ge<sub>3+x</sub>, where the bond order is fractional, with the hexagonal  $[Ge_6]^{10-}$  units showing characteristics of Hückel-aromaticity. <sup>50</sup> Examples of intermediate bond order in stannides also exist, with Ca<sub>9-x</sub>Li<sub>2</sub>Sn<sub>10</sub> being just a more recent one. <sup>70</sup>

One can surmise that in all structures,  $\pi^*$ -contributions to the Ge–Ge bond are expected to increase with increasing the Li content. A certain degree of covalency of the Li–Ge / Li–Li interactions, which the Zintl formalism does not capture, must also be considered to account more closely for the observed trend with regard to the distances. Similarly, bond lengths within the Sn<sub>2</sub> dumbbells in Li<sub>5-x</sub>Sn<sub>2+x</sub> phases can also be correlated to valence electron count. As seen from the refined distances, values of  $d_{\text{Sn-Sn}}$  are on the order of 2.86 Å. The Li<sub>13</sub>Sn<sub>5</sub> phase is another example having Sn–Sn dumbbells which crystallizes in trigonal crystal system with space group  $P \, \overline{3} m 1$ , <sup>36</sup> with  $d_{\text{Sn-Sn}}$  value of 2.864(7) Å. Li<sub>5-x</sub>Sn<sub>2+x</sub> and Li<sub>13</sub>Sn<sub>5</sub> have ~2.4 and 2.6 electrons donated to each Sn atom, respectively. For comparison, the structure of the lithium richer stannide Li<sub>7</sub>Sn<sub>2</sub> (3.5 electrons donated to each Sn) shows Sn–Sn dumbbells that are stretched to  $d_{\text{Sn-Sn}} = 2.999(7)$  Å. <sup>35</sup> The experimental crystal structure of the Li<sub>7</sub>Sn<sub>3</sub> phase (Li/Sn = 2.33) <sup>33</sup> does not match that of the computationally predicted Li<sub>7</sub>Ge<sub>3</sub>, despite the same composition. There are bent Sn<sub>3</sub>-fragments

in  $\text{Li}_7\text{Sn}_3$  (Figure S5) with  $d_{\text{Sn-Sn}}$  of 2.943(3) Å, which may indicate that Sn–Sn interaction in this stannide, akin to a single bond, ought to correspond to Sn–Sn distance of about 2.9 Å or longer.

Another important observation regarding distances here concerns the disorder in  $\text{Li}_{\text{S-x}}\text{Sn}_{2+x}$ , which was modeled as statistical admixing of Li and Sn atoms. This means that in the case where tin atoms partially replace lithium atoms, more convoluted atomic bonding results and one needs to consider the formation of larger covalently-bonded fragments of tin. The exact nature of those polyanions is unclear since the refinement suggest up to ca. 8:1 ratio of Li:Sn (Table 3). Nevertheless, the lithium atoms which are partially replaced by tin atoms and their neighboring atoms will be interacting in a more covalent fashion, which becomes evident from the distances (Li1/Sn)–Sn, which are ca. 2.75 Å long. Such value is close to the sum of the covalent radii ( $r_{\text{Li}} = 1.28 \text{ Å}$ ,  $r_{\text{Sn}} = 1.44 \text{ Å}$ ).<sup>69</sup> Considering the refined proportions, the expected single bond distance can be estimated as [(0.88×  $r_{\text{Li}}$ ) + (0.12×  $r_{\text{Sn}}$ ) +  $r_{\text{Sn}} = 2.73 \text{ Å}$ ]. For comparison, distances involving the lithium atoms that are not disordered (Li2 and Li3) are ca. 2.8 Å and longer.

#### 3.5. Electronic structure

Electronic structure calculations were carried out for the idealized (disorder-free) Li<sub>5</sub>Ge<sub>2</sub> and Li<sub>5</sub>Sn<sub>2</sub>, as well as for ordered models with the compositions Li<sub>14</sub>Ge<sub>6</sub> (derived from the refined composition Li<sub>247</sub>Ge<sub>2</sub>; Table 1) and Li<sub>14</sub>Sn<sub>7</sub> (derived from the refined composition Li<sub>248</sub>Sn<sub>22</sub>; Table 3). The former model was constructed by removing one of the three Li3 atoms (Wyckoff site 3*a*) from the conventional rhombohedral unit cell of Li<sub>5</sub>Ge<sub>2</sub>. The latter model was generated by replacing one of the six Li1 atoms (Wyckoff site 6*c*) by Sn in the conventional rhombohedral unit cell of Li<sub>5</sub>Sn<sub>2</sub>. The resulting composition, Li<sub>4.7</sub>Sn<sub>2.3</sub>, is somewhat richer in Sn than the experimentally determined composition but a more reasonably proxy of the chemical bonding relative to Li<sub>5</sub>Sn<sub>2</sub>.

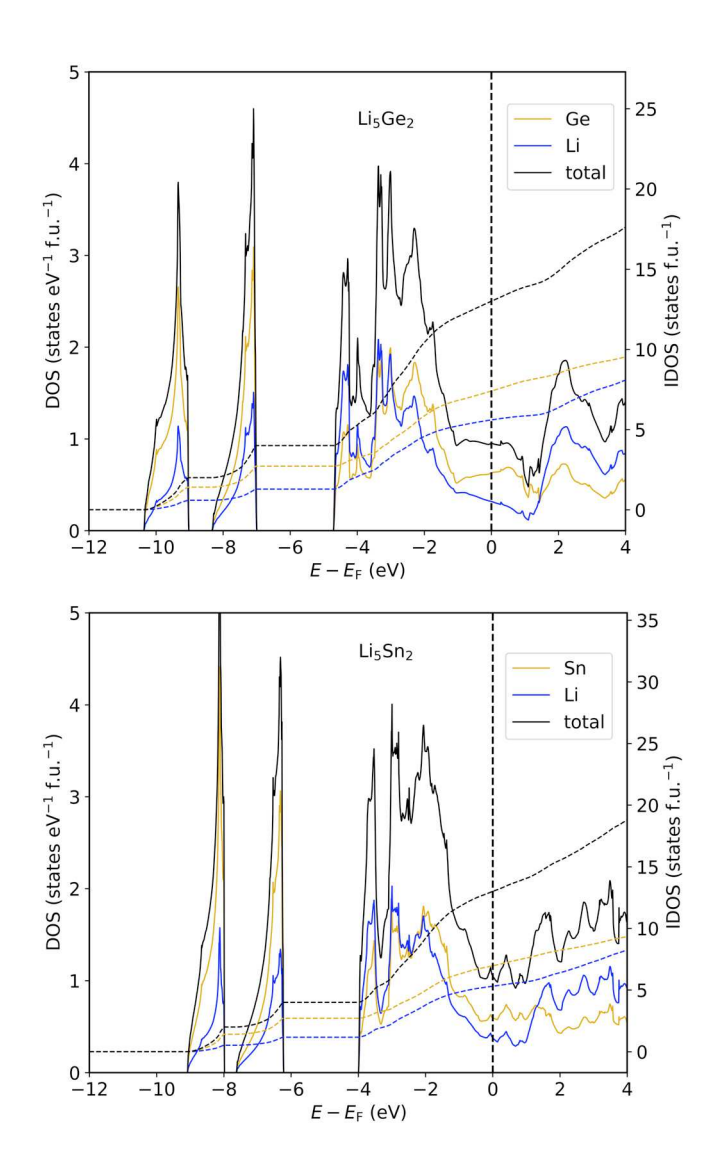


Figure 7. Total and projected densities of states for the idealized compositions Li<sub>5</sub>Ge<sub>2</sub> and Li<sub>5</sub>Sn<sub>2</sub>.

Total and projected densities of states for the idealized compositions Li<sub>5</sub>Ge<sub>2</sub> and Li<sub>5</sub>Sn<sub>2</sub> are shown in Figure 7. Both compounds reveal metallic behavior with no discernible (pseudo)gaps in the vicinity of the Fermi level. The observed picture is different from that in other electronically imprecise Zintl phases, where actual gaps or dips in the density of states are observed at the electron count corresponding to the charge-balanced composition. A possible explanation of the observed discrepancy is the combination of the rather covalent character of the Li–Ge bonding and the presence of short Li–Li distances. Both these

factors drive the system away from the ideal Zintl picture where electrons are donated by the electropositive atoms to the polyanions consisting of electronegative atoms. Analysis of the charge distribution within Bader's Quantum Theory of Atoms in Molecules, done by integrating the valence electron density inside the all-electron density basins, produces the following Bader charges for the two compounds: Li1 (+0.81), Li2 (+0.81), Li3 (+0.83), Ge (-2.03) for Li<sub>5</sub>Ge<sub>2</sub> and Li1 (+0.81), Li2 (+0.82), Li3 (+0.83), Sn (-2.04) for Li<sub>5</sub>Sn<sub>2</sub>. These values show a significant degree of covalency for the Li–Ge and Li–Sn bonding, as indicated by the incomplete electron transfer from the Li atoms. Taking into account the fact that absolute values of Bader charges are expected to be lower than the ideal ionic charges, it is evident that the calculated Bader charges for Ge and Sn in Li<sub>5</sub> $Tt_2$  lie between the expected formal charges for single- and double-bonded Tt species.

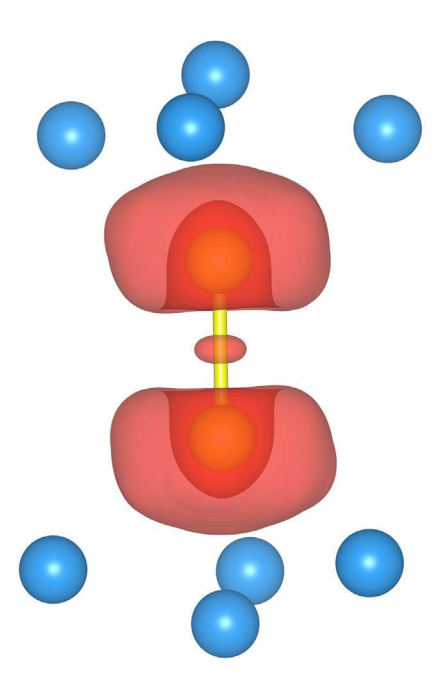


Figure 8. A fragment of the idealized Li<sub>5</sub>Ge<sub>2</sub> crystal structure with the Electron Localization Function (ELF) shown at the 0.7 isosurface level.

The most prominent features of the Electron Localization Function (ELF) for both  $\text{Li}_5\text{Ge}_2$  and  $\text{Li}_5\text{Sn}_2$  are the clear maxima between the Tt atoms, corresponding to the Tt–Tt bonding, as well as the lone-pair features in the vicinity of the Tt atoms (Figure 8, shown here for a fragment of the  $\text{Li}_5\text{Ge}_2$  crystal structure at the 0.7 isosurface level). Integration of the valence electron density in the ELF basins yields 0.52 and 0.49 electrons for the Tt–Tt bond attractor in  $\text{Li}_5\text{Ge}_2$  and  $\text{Li}_5\text{Sn}_2$ , respectively, pointing toward considerable degree of delocalization of the chemical bonding, not unusual for metals.

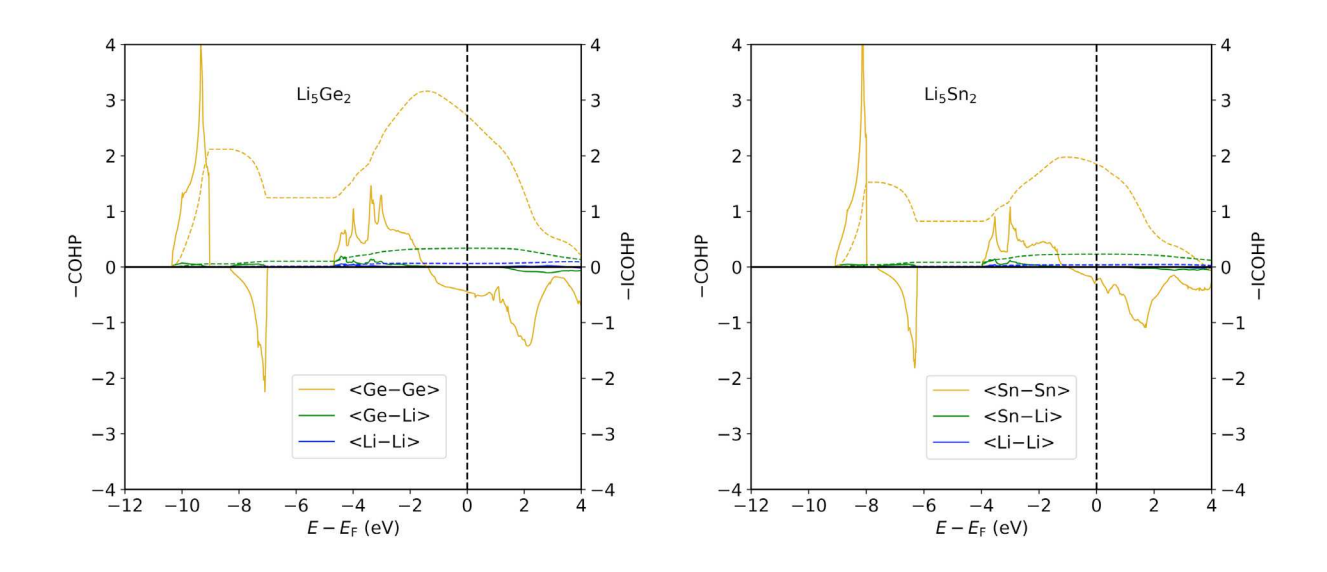


Figure 9. Crystal orbital Hamilton population (COHP) curves for averaged *Tt–Tt*, *Tt–*Li and Li–Li interactions in idealized compositions Li<sub>5</sub>Ge<sub>2</sub> and Li<sub>5</sub>Sn<sub>2</sub>.

Crystal Orbital Hamilton Population curves (COHP) for  $\text{Li}_5\text{Ge}_2$  and  $\text{Li}_5\text{Sn}_2$  are shown in Figure 9. Both compounds exhibit similar bonding features: the strongest bonds (in terms of the integrated COHP per bond) are the Tt-Tt bonds, which are underoptimized at the Fermi level due to population of some antibonding states. This means that these interactions favor hole doping. In contrast, Li-Tt and Li-Li interactions are essentially optimized at  $E_F$ . Furthermore, due to the Li-Tt and Li-Li bonding and

antibonding interactions being balanced out in a wide energy range around the Fermi level, these interactions should be stable with respect to both hole and electron doping.

Analysis of the COHP characteristics for a hypothetical ordered Li<sub>4.7</sub>Ge<sub>2</sub> structure (a model for the experimentally observed composition), qualitatively confirms the conclusions derived from the electronic structure of the idealized Li<sub>5</sub>Ge<sub>2</sub> (Figure S6). Since removal of a small amount of Li can be effectively viewed as hole doping, it is not surprising that the electronic structure of Li<sub>4.7</sub>Ge<sub>2</sub> resembles that of Li<sub>5</sub>Ge<sub>2</sub>, but with the Fermi level slightly shifted down. While this shift has a somewhat stabilizing effect on the Ge–Ge bonding, a complete optimization of the Ge–Ge interactions is expected to be achieved at the composition Li<sub>3.6</sub>Ge<sub>2</sub>, i.e., with the Fermi level shifted down to the top of the bonding state domain. However, such a Li-deficient composition may not be experimentally realizable, due to potential collapse of the structure.

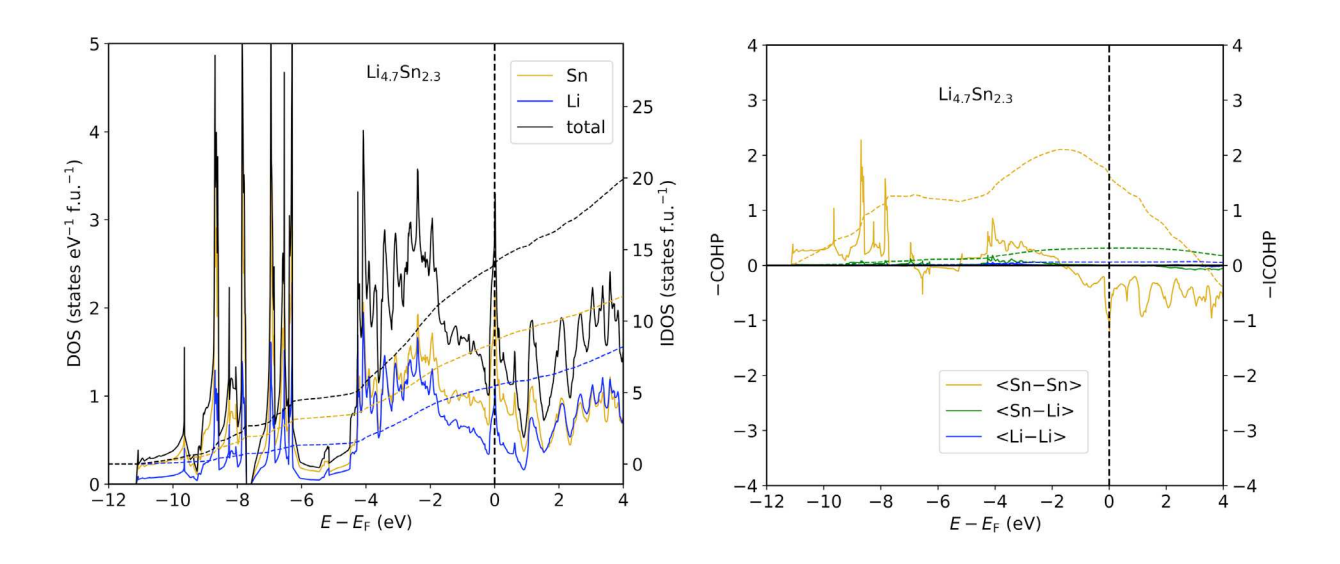


Figure 10. Calculated total and projected densities of states for Li<sub>4.7</sub>Sn<sub>2.3</sub> (left) and Crystal orbital Hamilton population (COHP) curves for Sn–Sn, Sn–Li and Li–Li interactions in Li<sub>4.7</sub>Sn<sub>2.3</sub> (right).

A notably different picture is observed for the phase with Li/Sn disorder, Li<sub>4.7</sub>Sn<sub>2.3</sub>, modeled by an ordered super-structure. Here, the departure from the ideal stoichiometry results in an apparent electron doping (Figure 10), which can be also easily understood by consideration of the formal charges: Replacement of one Li atom by Sn, would result in a formal charge of 0 for this introduced Sn atom, since it would be bonded to four Sn neighbors. However, for the four Sn atoms in the coordination environment of this substituted position, the formal negative charge will be reduced (by absolute value) due to the increase of their covalent bond count, so that the overall effect is indeed electron doping. Although electron doping is expected to have a destabilizing effect on the Sn–Sn bonds, this kind of compositional change also increases the total number of the Sn–Sn bonds in the structure, which seems to counteract the destabilization. We would also like to note that, due to the higher Sn content in the employed model in comparison with the experimental composition, the Fermi level in Li<sub>4.7</sub>Sn<sub>2.3</sub> crosses a peak in the electronic density of states. For the experimental composition, the Fermi level is expected to be located just below the peak.

Thus, one can conclude that non-stoichiometry in  $\text{Li}_5Tt_2$  can be accompanied by both hole and electron doping. The former scenario results in the stabilization of the Tt-Tt bonding and can be achieved by creating Li vacancies in the structure, while the latter case involves replacement of Li by Tt, which, despite having a destabilizing effect on the Tt-Tt interactions, increases the total number of the Tt-Tt contacts. At the moment, it is not possible to say which scenario will be favorable in each particular case, since another important parameter, namely the geometric distortions of the crystal structures upon different disorder realizations, has not been considered and will require additional experimental and theoretical work.

## 4. CONCLUSIONS

Lithium forms a number of binary and ternary germanides and stannides with unique structures. Many of them exhibit complex bonding characteristics, and elude proper rationalization by the Zintl-Klemm concept. Here we revisited the relatively simple structures of the  $\text{Li}_5Tt_2$  (Tt = Ge, Sn) phases based on single-crystal X-ray diffraction data, together with Rietveld refinements of synchrotron X-ray powder diffraction and neutron powder diffraction data. By combination of all three methods, we found Li/Sn disorder in  $\text{Li}_5\text{Sn}_2$ , resulting in final chemical formula of  $\text{Li}_{5-x}\text{Sn}_{2+x}$  (0 < x < 0.15). In contrats, for the germanide analog, vacancies on one of the Li sites in  $\text{Li}_5\text{Ge}_2$  were identified, which results in the final chemical formula of  $\text{Li}_{5-x}\text{Ge}_2$  ( $x \approx 0.3$ ).

The off-stoichiometry and the concomitant varied electron count were found to be in correlation with the change of bond order within the  $[Tt_2]$  dimers. The latter is evidenced by the change in bond lengths and the clear the variation of the  $\pi$ -antibonding characteristics. The bond order of  $[Ge_2]$  is neither 1 nor 2, which can be inferred from the Zintl reasoning that suggested the following partitioning scheme of valence electrons  $(Li^+)_{4,7}$   $[Ge_2]^{4,7-}$ . The lone-pair features of the  $[Tt_2]$  anions are also corroborated from the Electron Localization Function (ELF) calculations.

Analogous structural motifs and chemical bonding is present in the structures of the  $\text{Li}_7Tt_2$  (Tt = Ge, Sn) phases, raising the question on possible disorder in the latter cases. Since we found that the Zintl concept is applicable to understanding the chemical bonding in  $\text{Li}_{5-x}\text{Sn}_{2+x}$  and  $\text{Li}_{5-x}\text{Ge}_2$ , at least at a basic level, it will be interesting to see if it will yield the same results for the Li-richer phases. In that note, we recall that the Zintl concept could not provide deeper insights as to why the stannide with the "5-2" structure exhibits Li/Sn disorder, while Li-defects exist for the germanide. Therefore, follow-up work studying  $\text{Li}_{7-x}Tt_{2+x}$  vs  $\text{Li}_{7-x}Tt_2$  scenarios is anticipated to shed more light on this problem.

#### ASSOCIATED CONTENT

# **Supporting Information.**

The Supporting information is available free of charge at <a href="https://pubs.acs.org/doi/">https://pubs.acs.org/doi/</a>

Experimental plots of synchrotron X-ray powder diffraction (SXPD) and neutron powder diffraction (NPD) patterns of  $\text{Li}_{5-x}\text{Sn}_{2+x}$  and  $\text{Li}_{5-x}\text{Ge}_2$  (Figure S1, S2); Table with a summary of experimental results in terms of nominal compositions and major phases detected by powder X-ray diffraction (Table S1); Refined atomic coordinates for  $\text{Li}_{5-x}\text{Sn}_{2+x}$  and  $\text{Li}_{5-x}\text{Ge}_2$  (Table S2, S3); schematic representation of the puckered hexagonal sheets of Li atoms in the structure of  $\text{Li}_{5-x}\text{Ge}_2$  (Figure S3); schematic representation of the rhombohedral  $\text{BaLi}_2\text{In}_2\text{Ge}_2$  and  $\text{Li}_5\text{Ge}_2$  structures showing them as isotypic (Pearson symbol hR7, Wyckoff  $b^3a$ ) (Figure S4); representation of the crystal structure of the monoclinic  $\text{Li}_7\text{Sn}_3$  phase (Figure S5); densities of states and COHP curves for  $\text{Li}_{47}\text{Ge}_2$  (Figure S6).

## **AUTHOR INFORMATION**

# **Corresponding Author**

\* **Svilen Bobev** – Department of Chemistry and Biochemistry, University of Delaware, Newark, Delaware 19716, United States; <a href="http://orcid.org/0000-0002-0780-4787">http://orcid.org/0000-0002-0780-4787</a>; Email: <a href="mailto:bobev@udel.edu">bobev@udel.edu</a>

## **Authors**

**Kowsik Ghosh** – Department of Chemistry and Biochemistry, University of Delaware, Newark, Delaware 19716, United States;

**Salina Rahman** – Department of Chemistry and Biochemistry, University of Delaware, Newark, Delaware 19716, United States;

**Alexander Ovchinnikov** – Department of Chemistry and Biochemistry, University of Delaware, Newark, Delaware 19716, United States; Faculty of Chemistry and Food Chemistry, Technische Universität Dresden, 01062 Dresden, Germany

## **Author Contributions**

The manuscript was written through contributions of all authors. All authors have given approval to the final version of the manuscript.

# **Funding Sources**

The authors acknowledge financial support from the US National Science Foundation (NSF) through grant DMR-2004579.

# Acknowledgement

We give sincere thanks to Dr. Alicia Manjon Sanz at the Spallation Neutron Source of the Oak National Laboratory, USA for collecting neutron powder diffraction data. We also thank Dr. Graham King from the Canadian Light Source, Canada for collecting Synchrotron X-ray powder diffraction data.

#### **Notes**

The authors declare no competing financial interest.

# REFERENCES

- (1) Goodenough, J. B.; Park, K. S. The Li-Ion Rechargeable Battery: A Perspective. *J. Am. Chem. Soc.* **2013**, *135*, 1167–1176. https://doi.org/10.1021/ja3091438.
- (2) Manthiram, A. A Reflection on Lithium-Ion Battery Cathode Chemistry. *Nat. Commun.* **2020**, *11*, 1–9. https://doi.org/10.1038/s41467-020-15355-0.
- (3) Ma, D.; Cao, Z.; Hu, A. Si-Based Anode Materials for Li-Ion Batteries: A Mini Review. *Nano-Micro Lett.* **2014**, *6*, 347–358. https://doi.org/10.1007/s40820-014-0008-2.
- (4) Kim, T.; Song, W.; Son, D. Y.; Ono, L. K.; Qi, Y. Lithium-Ion Batteries: Outlook on Present, Future, and Hybridized Technologies. *J. Mater. Chem. A* **2019**, 7, 2942–2964. https://doi.org/10.1039/C8TA10513H.
- (5) Nitta, N.; Wu, F.; Lee, J. T.; Yushin, G. Li-Ion Battery Materials: Present and Future. *Mater. Today* **2015**, *18*, 252–264. https://doi.org/10.1016/j.mattod.2014.10.040.
- (6) Weiss, M.; Ruess, R.; Kasnatscheew, J.; Levartovsky, Y.; Levy, N. R.; Minnmann, P.; Stolz, L.; Waldmann, T.; Wohlfahrt-Mehrens, M.; Aurbach, D.; Winter, M.; Ein-Eli, Y.; Janek, J. Fast Charging of Lithium-Ion Batteries: A Review of Materials Aspects. *Adv. Energy Mater.* **2021**, *11*, 2101126. https://doi.org/10.1002/aenm.202101126.
- (7) Manthiram, A. An Outlook on Lithium Ion Battery Technology. *ACS Cent. Sci.* **2017**, *3*, 1063–1069. https://doi.org/10.1021/acscentsci.7b00288.
- (8) Hayner, C. M.; Zhao, X.; Kung, H. H. Materials for Rechargeable Lithium-Ion Batteries. *Annu. Rev. Chem. Biomol. Eng.* **2012**, *3*, 445–471. https://doi.org/10.1146/annurev-chembioeng-062011-081024.
- (9) Shukla, A. K.; Kumar, T. P. Lithium Economy: Will It Get the Electric Traction? *J. Phys. Chem. Lett.* **2013**, *4*, 551–555. https://doi.org/10.1021/jz3013497.

- (10) Scrosati, B.; Hassoun, J.; Sun, Y. K. Lithium-Ion Batteries. *A Look into the Future. Energy Environ. Sci.* **2011**, *4*, 3287–3295. https://doi.org/10.1039/c1ee01388b.
- (11) Etacheri, V.; Marom, R.; Elazari, R.; Salitra, G.; Aurbach, D. Challenges in the Development of Advanced Li-Ion Batteries: A Review. *Energy Environ*. *Sci.* **2011**, *4*, 3243–3262. https://doi.org/10.1039/c1ee01598b.
- (12) Lim, L. Y.; Liu, N.; Cui, Y.; Toney, M. F. Understanding Phase Transformation in Crystalline Ge Anodes for Li-Ion Batteries. *Chem. Mater.* **2014**, *26*, 3739–3746. https://doi.org/10.1021/cm501233k.
- (13) Park, C. M.; Kim, J. H.; Kim, H.; Sohn, H. J. Li-Alloy Based Anode Materials for Li Secondary Batteries. *Chem. Soc. Rev.* **2010**, *39*, 3115–3141. https://doi.org/10.1039/b919877f.
- (14) Lee, S. S.; Nam, K. H.; Jung, H.; Park, C. M. Si-Based Composite Interconnected by Multiple Matrices for High-Performance Li-Ion Battery Anodes. *Chem. Eng. J.* **2020**, *381*, 122619. https://doi.org/10.1016/j.cej.2019.122619.
- (15) Mukanova, A.; Jetybayeva, A.; Myung, S.; Kim, S.; Bakenov, Z. A Mini-Review on the Development of Si-Based Thin Film Anodes for Li-Ion Batteries. *Mater. Today Energy* **2018**, *9*, 49–66. https://doi.org/10.1016/j.mtener.2018.05.004.
- (16) Ko, M.; Chae, S.; Cho, J. Challenges in Accommodating Volume Change of Si Anodes for Li-Ion Batteries. *ChemElectroChem* **2015**, 2, 1645–1651. https://doi.org/10.1002/celc.201500254.
- (17) Sun, P.; Davis, J.; Cao, L.; Jiang, Z.; Cook, J. B.; Ning, H.; Liu, J.; Kim, S.; Fan, F.; Nuzzo, R.
  G.; Braun, P. V. High Capacity 3D Structured Tin-Based Electroplated Li-Ion Battery Anodes. *Energy Storage Mater.* 2019, 17, 151–156. https://doi.org/10.1016/j.ensm.2018.11.017.

- (18) Teki, R.; Krishnan, R.; Parker, T. C.; Lu, T. M.; Datta, M. K.; Kumta, P. N.; Koratkar, N. Nanostructured Silicon Anodes for Lithium Ion Rechargeable Batteries. *Small* **2009**, *5*, 2236–2242. https://doi.org/10.1002/smll.200900382.
- (19) Pell, E. M. Solubility of Lithium in Germanium. *J. Phys. Chem. Solids* **1957**, *3*, 74–76. https://doi.org/10.1016/0022-3697(57)90050-1.
- (20) Menges, E.; Hopf, V.; Schäfer, H.; Weiss, A. Die Kristallstruktur von LiGe Ein Neuartiger, Dreidimensionaler Verband von Element(IV)-Atomen. Z. Naturforsch. B 1969, 24, 1351–1352. https://doi.org/10.1515/znb-1969-1034.
- (21) Hopf, V.; Schäfer, H.; Weiss, A. Die Kristallstruktur Der Phase Li<sub>9</sub>Ge<sub>4</sub>. Z. Naturforsch. B **1970**, 25, 653. https://doi.org/10.1515/znb-1970-0624.
- (22) Hopf, V.; Müller, W.; Schäfer, H. The Structure of Li<sub>7</sub>Ge<sub>2</sub>. Z. Naturforsch. B **1972**, 27, 1157–1160. https://doi.org/10.1515/znb-1972-1009.
- (23) Frank, U.; Müller, W. Li<sub>11</sub>Ge<sub>6</sub> Eine Phase Mit Isolierten, Ebenen Ge-Fünfringen. *Z. Naturforsch*. *B* **1975**, *30*, 313–315. https://doi.org/10.1515/znb-1975-5-604.
- (24) Kiefer, F.; Fässler, T. F. Synthesis and Revised Structure of the Zintl Phase Li<sub>7</sub>Ge<sub>12</sub>. *Solid State Sci.* **2011**, *13*, 636–640. https://doi.org/10.1016/j.solidstatesciences.2010.12.038.
- (25) Zeilinger, M.; Fässler, T. F. Structural and Thermodynamic Similarities of Phases in the Li–Tt (Tt = Si, Ge) Systems: Redetermination of the Lithium-Rich Side of the Li–Ge Phase Diagram and Crystal Structures of  $\text{Li}_{17}\text{Si}_{4.0-x}\text{Ge}_x$  for x = 2.3, 3.1, 3.5, and 4 as well as  $\text{Li}_{4.1}\text{Ge}$ . *Dalton Trans.* **2014**, *43*, 14959–14970. https://doi.org/10.1039/c4dt00743c.

- (26) Goward, G. R.; Taylor, N. J.; Souza, D. C. S.; Nazar, L. F. The True Crystal Structure of  $\text{Li}_{17}\text{M}_4$  (M = Ge, Sn, Pb)–Revised from  $\text{Li}_{22}\text{M}_5$ . J. Alloys Compd. **2001**, 329, 82–91. https://doi.org/10.1016/S0925-8388(01)01567-5.
- (27) Osman, H. H.; Bobev, S. Experimental and Theoretical Study on the Substitution Patterns in Lithium Germanides: The Case of Li<sub>15</sub>Ge<sub>4</sub> vs Li<sub>14</sub>ZnGe<sub>4</sub>. *Eur. J. Inorg. Chem.* **2022**, e202100901. https://doi.org/10.1002/ejic.202100901.
- (28) Johnson, Q.; Smith, G. S.; Wood, D. The Crystal Structure of Li<sub>15</sub>Ge<sub>4</sub>. *Acta Crystallogr*. **1965**, *18*, 131–132. https://doi.org/10.1107/s0365110x65000257.
- (29) Scherf, L. M.; Riphaus, N.; Fässler, T. F. Site-Specific Substitution Preferences in the Solid Solutions Li<sub>12</sub>Si<sub>7-x</sub>Ge<sub>x</sub>, Li<sub>12-y</sub>Na<sub>y</sub>Si<sub>7</sub>, Na<sub>7</sub>LiSi<sub>8-z</sub>Ge<sub>z</sub>, and Li<sub>3</sub>NaSi<sub>6-y</sub>Ge<sub>y</sub>. Z. Anorg. Allg. Chem. **2016**, 642, 1143–1151. https://doi.org/10.1002/zaac.201600259.
- (30) Dopilka, A.; Childs, A.; Bobev, S.; Chan, C. K. Understanding the Amorphous Lithiation Pathway of the Type I Ba<sub>8</sub>Ge<sub>43</sub> Clathrate with Synchrotron X-Ray Characterization. *Chem. Mater.* **2020**, 32, 9444–9457. https://doi.org/10.1021/acs.chemmater.0c03641.
- (31) Hansen, D. A.; Chang, L. J. Crystal Structure of Li<sub>2</sub>Sn<sub>5</sub>. *Acta Crystallogr. B* **1969**, 25, 2392–2395. https://doi.org/10.1107/s0567740869005760.
- (32) Müller, W.; Schäfer, H. Die Kristallstruktur Der Phase LiSn: The Crystal Structure of LiSn. Z. *Naturforsch. B* **1973**, 28, 246–248. https://doi.org/10.1515/znb-1973-5-604.
- (33) Müller, W. Preparation And Crystal Structure of Li<sub>7</sub>Sn<sub>3</sub>. Z. Naturforsch. B **1974**, 29, 304–311. https://doi.org/10.1515/znb-1974-5-602.
- (34) Frank, U.; Müller, W.; Schäfer, H. Die Struktur Der Phase Li<sub>5</sub>Sn<sub>2</sub>. Z. Naturforsch. B **1975**, 30, 1–5. https://doi.org/10.1515/znb-1975-1-202.

- (35) Frank, U.; Müller, W.; Schäfer, H. Die Kristallstruktur Der Phase Li<sub>7</sub>Sn<sub>2</sub>. Z. Naturforsch. B **1975**, 30, 6–9. https://doi.org/10.1515/znb-1975-1-203.
- (36) Frank, U.; Müller, W. Darstellung Und Struktur Der Phase Li<sub>13</sub>Sn<sub>5</sub> Und Die Strukturelle Verwandtschaft Der Phasen in Den Systemen Li-Sn Und Li-Pb. Z. Naturforsch. B **1975**, 30, 316–322. https://doi.org/10.1515/znb-1975-5-605.
- (37) Dahn, J. R.; Courtney, I. A.; Mao, O. Short-range Sn ordering and crystal structure of Li<sub>4.4</sub>Sn prepared by ambient temperature electrochemical methods. *Solid State Ion.* **1998**, *111*, 289–294. https://doi.org/10.1016/S0167-2738(98)00175-1.
- (38) Hahn, C.; Mao, J. G.; Rabalais, J. W.; Guloy, A. M.; Richardson, J. W. X-Ray and Neutron Diffraction Studies on "Li<sub>4.4</sub>Sn." *Inorg. Chem.* **2003**, *42*, 3765–3771. https://doi.org/10.1021/ic0262350.
- (39) Stelzer, R. U.; Ikeda, Y.; Srinivasan, P.; Lehmann, T. S.; Grabowski, B.; Niewa, R. Li₅Sn, the Most Lithium-Rich Binary Stannide: A Combined Experimental and Computational Study. *J. Am. Chem. Soc.* **2022**, *144*, 7096–7110. https://doi.org/10.1021/jacs.1c10640.
- (40) Hao, C. M.; Li, Y.; Zhu, Q.; Chen, X. Y.; Wang, Z. X.; Li, Y. L. Pressure-Induced Structural Phase Transition in Li<sub>4</sub>Ge. *CrystEngComm* **2018**, *20*, 5949–5954. https://doi.org/10.1039/c8ce00783g.
- (41) Evers, J.; Oehlinger, G. Isolated Hexagonal Channels Built up by Three-Connected Ge- Ions in LiGe at High Pressure. *Angew. Chem. Int. Ed.* **2001**, *40*, 1050–1053. https://doi.org/10.1002/1521-3773(20010316)40:6<1050::AID-ANIE10500>3.0.CO;2-J.
- (42) Schäfer, H.; Axel, H.; Menges, E.; Weiss, A. Zur Kenntnis Des Systems Lithium-Silicium. Z. *Naturforsch. B* **1965**, 20 394. https://doi.org/10.1515/znb-1965-0427.
- (43) Frank, U.; Müller, W.; Schäfer, H. Zur Kenntnis Der Phase Li<sub>13</sub>Si<sub>4</sub> / On The Phase Li<sub>13</sub>Si<sub>4</sub>. Z. *Naturforsch. B* **1975**, *30*, 10–13. https://doi.org/10.1515/znb-1975-1-204.

- (44) Zeilinger, M.; Fässler, T. F. Revision of the Li<sub>13</sub>Si<sub>4</sub> Structure. *Acta Crystallogr. E* **2013**, *69*, 81–82. https://doi.org/10.1107/S1600536813029759.
- (45) Nesper, R. Structure and chemical bonding in Zintl phases containing lithium. *Prog. Solid St. Chem.* **1990**, *20*, 1–45. https://doi.org/10.1016/0079-6786(90)90006-2.
- (46) Nesper, R.; Curda, J.; Von Schnering, H. G. Li<sub>8</sub>MgSi<sub>6</sub>, a Novel Zintl Compound Containing Quasi-Aromatic Si<sub>5</sub> Rings. *J. Solid State Chem.* **1986**, 62, 199–206. https://doi.org/10.1016/0022-4596(86)90232-X.
- (47) Morris, A. J.; Grey, C. P.; Pickard, C. J. Thermodynamically Stable Lithium Silicides and Germanides from Density Functional Theory Calculations. *Phys. Rev. B* **2014**, *90*, 22–24. https://doi.org/10.1103/PhysRevB.90.054111.
- (48) von Schnering, H.-G.; Nesper, R.; Tebbe, K. F.; Curda, J. Struktur Und Eigenschaften von Li<sub>14</sub>Si<sub>6</sub> (Li<sub>2 33</sub>Si), Der Violetten Phase Im System Lithium-Silicium. *Z. Met.* **1980**, *71*, 357–363.
- (49) Ghosh, K.; Ovchinnikov, A.; Baitinger, M.; Krnel, M.; Burkhardt, U.; Grin, Y.; Bobev, S. Lithium Metal Atoms Fill Vacancies in the Germanium Network of a Type-I Clathrate: Synthesis and Structural Characterization of Ba<sub>8</sub>Li<sub>5</sub>Ge<sub>41</sub>. *Dalton Trans*. **2023**, 52, 10310–10322. https://doi.org/10.1039/d3dt01168b.
- (50) Ghosh, K.; Bobev, S. Yet Another Case of Lithium Metal Atoms and Germanium Atoms Sharing Chemistry in the Solid State: Synthesis and Structural Characterization of Ba<sub>2</sub>LiGe<sub>3</sub>. *Chem. Eur. J.* **2023**, 202302385, 1–10. https://doi.org/10.1002/chem.202302385.
- (51) Kauzlarich, S. M. Chemistry, Structure and Bonding of Zintl Phases and Ions. *VCH*, *New York* **1998**.

- (52) Nesper, R. The Zintl-Klemm Concept A Historical Survey. Z. Anorg. Allg. Chem. **2014**, 640, 2639–2648. https://doi.org/10.1002/zaac.201400403.
- (53) Sheldrick, G. M. SHELXT Integrated Space-Group and Crystal-Structure Determination. *Acta Crystallogr*. A **2015**, 71, 3–8. https://doi.org/10.1107/S2053273314026370.
- (54) Sheldrick, G. M. Crystal Structure Refinement with SHELXL. *Acta Crystallogr. C* **2015**, *71*, 3–8. https://doi.org/10.1107/S2053229614024218.
- (55) Akselrud, L. G.; Zavalii, P. Y.; Grin, Y. N.; Pecharski, V. K.; Baumgartner, B.; Wölfel, E. Use of the CSD Program Package for Structure Determination from Powder Data. *Mater. Sci. Forum* **1993**, *133*–136, 335–342. https://doi.org/10.4028/www.scientific.net/msf.133-136.335.
- (56) Toby, B. H. EXPGUI, a Graphical User Interface for GSAS. J. Appl. Crystallogr. 2001, 34, 210–213. https://doi.org/10.1107/S0021889801002242.
- (57) Von Dreele, R. B.; Jorgensen, J. D.; Windsor, C. G. Rietveld Refinement with Spallation Neutron Powder Diffraction Data. *J. Appl. Crystallogr.* **1982**, *15*, 581–589. https://doi.org/10.1107/s0021889882012722.
- (58) Andersen, O. K. Linear Methods in Band Theory. *Phys. Rev. B* **1975**, *12*, 3060–3083. https://doi.org/10.1080/00431672.1975.9931783.
- (59) Andersen, O. K.; Jepsen, O. Explicit, First-Principles Tight-Binding Theory. *Phys. Rev. Lett.* **1984**, *53*, 2571–2574. https://doi.org/10.1103/PhysRevLett.53.2571.
- (60) von Barth, U.; Hedin, L. A Local Exchange-Correlation Potential for the Spin Polarized Case. I. J. *Phys. C Solid State Phys.* **1972**, *5*, 1629–1642. https://doi.org/10.1088/0022-3719/5/13/012.
- (61) Savin, A.; Nesper, R.; Wengert, S.; Fässler, T. F. ELF: The Electron Localization Function. Angew. Chem., Int. Ed. Engl. 1997, 36, 1808–1832, https://doi.org/10.1002/anie.199718081.

- (62) Otero-de-la-Roza, A.; Johnson, E. R.; Luaña, V. Critic2: A Program for Real-Space Analysis of Quantum Chemical Interactions in Solids. *Comput. Phys. Commun.* **2014**, *185*, 1007–1018, https://doi.org/10.1016/j.cpc.2013.10.026.
- (63) Baranets, S.; He, H.; Bobev, S. Niobium-bearing Arsenides and Germanides from Elemental Mixtures not Involving Niobium: A New Twist to an Old Problem in Solid-state Synthesis. *Acta Crystallogr. C* **2018**, 74, 623. doi: 10.1107/S2053229618005739.
- (64) Liang, Y.; Carrillo-Cabrera, W.; Ormeci, A.; Böhme, B.; Baitinger, M.; Grin, Y. The  $2\times2\times2$  Superstructure in the Clathrate-I  $K_8Li_xGe_{44-x/4}\square_{2-3x/4}$ . Z. Anorg. Allg. Chem. **2015**, 641, 339–347. https://doi.org/10.1002/zaac.201400565.
- (65) Liang, Y.; Böhme, B.; Ormeci, A.; Borrmann, H.; Pecher, O.; Haarmann, F.; Schnelle, W.; Baitinger, M.; Grin, Y. A Clathrate-I Phase with Li-Ge Framework. *Chem. Eur. J.* **2012**, *18*, 9818–9822. https://doi.org/10.1002/chem.201202069.
- (66) Jung, H.; Allan, P. K.; Hu, Y., Borkiewicz, O. J.; Wang, X.; Han, W.; Du, L.; Pickard, C. J.; Chupas, P. J.; Chapman, K. W.; Morris, A. J.; Grey, C. P. Elucidation of the local and long-range structural changes that occur in germanium anodes in lithium-ion batteries. *Chem. Mater.* **2015**, 27, 1031–1041. https://doi.org/10.1021/cm504312x.
- (67) Scherf, L. M.; Karttunen, A. J.; Pecher, O.; Magusin, P. C. M. M.; Grey, C. P.; Fässler T. F. [Ge<sub>2</sub>]<sup>4-</sup> dumbbells with very short Ge–Ge distances in the Zintl phase Li<sub>3</sub>NaGe<sub>2</sub>: A solid-state equivalent to molecular O<sub>2</sub>. *Angew. Chem. Int. Ed.* **2016**, *55*, 1075–1079. http://dx.doi.org/10.1002/anie.201508044.
- (68) Ovchinnikov, A.; Bobev, S. Layered quaternary germanides Synthesis and crystal and electronic structures of  $AELi_2In_2Ge_2$  (AE = Sr, Ba, Eu). *Inorg. Chem.* **2019**, *58*, 7895–7904. https://doi.org/10.1021/acs.inorgchem.9b00588.

- (69) Pauling, L. The Nature of the Chemical Bonding, 3rd Ed. Cornell Univ. Press Ithaca, NY, USA **1960**, 403. https://doi.org/10.1002/jps.3030300111.
- (70) Ovchinnikov, A.; Bobev, S. Multifaceted Sn–Sn bonding in the solid state. Synthesis and structural characterization of four new Ca–Li–Sn compounds. *Dalton Trans.* **2019**, *48*, 14398–14407. https://doi.org/10.1039/C9DT02803J.

# For Table of Contents Only

From comprehensive experimental work and DT calculations, it is established that Li/Sn disorder in  $\text{Li}_5\text{Sn}_2$  exists, resulting in a chemical formula of  $\text{Li}_{5-x}\text{Sn}_{2+x}$  (0 < x < 0.1). For the germanide analog, vacancies on one of the Li sites in  $\text{Li}_5\text{Ge}_2$  were identified, which results in the final chemical formula of  $\text{Li}_{5-x}\text{Ge}_2$  ( $x \approx 0.3$ ). The off-stoichiometry and the concomitant varied electron count are in correlation with the change of bond order within the [Ge<sub>2</sub>] and [Sn<sub>2</sub>] dimers.

